Can a regional-scale reduction of atmospheric CO₂ during the COVID-19 pandemic be detected from space? A case study for East China using satellite XCO₂ retrievals

5 Michael Buchwitz[1], Maximilian Reuter[1], Stefan Noël[1], Klaus Bramstedt[1], Oliver Schneising[1], Michael Hilker[1], Blanca Fuentes Andrade[1], Heinrich Bovensmann[1], John P. Burrows[1], Antonio Di Noia[2,3], Hartmut Boesch[2,3], Lianghai Wu[4], Jochen Landgraf[4], Ilse Aben[4], Christian Retscher[5], Christopher W. O'Dell[6], David Crisp[7]

[1]Institute of Environmental Physics (IUP), University of Bremen, 28334 Bremen, Germany

10 [2]Earth Observation Science, University of Leicester, LE1 7RH, Leicester, UK

[3]NERC National Centre for Earth Observation, LE1 7RH, Leicester, UK

[4]SRON Netherlands Institute for Space Research, 3584 CA Utrecht, The Netherlands

[5]Directorate of Earth Observation Programmes, European Space Agency (ESA), ESRIN, 00044 Frascati, Italy

[6]Cooperative Institute for Research in the Atmosphere, Colorado State University (CSU), Fort Collins, CO 80523, USA

15 [7]Jet Propulsion Laboratory (JPL), Pasadena, CA 91109, USA

Correspondence to: Michael Buchwitz (buchwitz@uni-bremen.de)

Abstract. The COVID-19 pandemic resulted in reduced anthropogenic carbon dioxide (CO₂) emissions during 2020 in large parts of the world. To investigate whether a regional-scale reduction of anthropogenic CO₂ emissions during the COVID-19

20 pandemic can be detected using space-based observations of atmospheric CO₂ we have analysed a small ensemble of OCO-2 and GOSAT satellite retrievals of column-averaged dry-air mole fractions of CO₂, i.e. XCO₂. We focus on East China and use a simple data-driven analysis method. We present estimates of the relative change of East China monthly emissions in 2020 relative to previous periods limiting the analysis to October to May periods to minimize the impact of biogenic CO₂ fluxes. The ensemble mean indicates an emission reduction by approximately 10% ± 10% in March and April 2020. However, our

25 results show considerable month-to-month variability and significant differences across the ensemble of satellite data products analysed. For example, OCO-2 suggests a much smaller reduction (~1-2% ± 2%). This indicates that it is challenging to reliably detect and to accurately quantify the emission reduction with current satellite data sets. There are several reasons for this including the sparseness of the satellite data but also the weak signal; the expected regional XCO₂ reduction is only on the order of 0.1-0.2 ppm. Inferring COVID-19 related information on regional-scale CO₂ emissions using current satellite XCO₂

30 retrievals likely requires, if at all possible, a more sophisticated analysis method including detailed transport modelling and considering *a priori* information on anthropogenic and natural CO₂ surface fluxes.

1 Introduction

Carbon dioxide (CO_2) is the most important anthropogenic greenhouse gas significantly contributing to global warming (IPCC, 2013). CO_2 has many natural and anthropogenic sources and sinks and our current understanding of them has significant gaps (e.g., Ciais et al., 2014; Chevallier et al., 2014; Reuter et al., 2017c; Crisp et al., 2018; Friedlingstein et al., 2019). Efforts are ongoing to improve the fundamental understanding of the global carbon cycle, to improve our ability to project future changes, and to verify the effectiveness of policies such as the Paris Agreement (https://unfccc.int/process-and-meetings/the-paris-agreement/the-paris-agreement, last access: 8-Sept-2020) aiming to reduce greenhouse gas emissions (e.g., Ciais et al., 2014, 2015; Pinty et al., 2017, 2019; Crisp et al., 2018; Matsunaga and Maksyutov, 2018; Janssens-Maenhout et al., 2020).

Retrievals of XCO_2 from the satellite sensors SCIAMACHY/ENVISAT (Burrows et al., 1995; Bovensmann et al., 1999; Reuter et al., 2010, 2011), TANSO-FTS/GOSAT (Kuze et al., 2016) and from the Orbiting Carbon Observatory-2 (OCO-2) satellite (Crisp et al., 2004; Eldering et al., 2017; O'Dell et al., 2012, 2018) have been used in recent years to obtain information on natural CO_2 sources and sinks (e.g., Basu et al., 2013; Chevallier et al., 2014, 2015; Reuter et al., 2014a, 2017c; Schneising et al., 2014; Houweling et al., 2015; Kaminski et al., 2017; Liu et al., 2017; Eldering et al., 2017; Yin et al., 2018; Palmer et al., 2019; Miller and Michalak, 2020), on anthropogenic CO_2 emissions (e.g., Schneising et al., 2008, 2013; Reuter et al., 2014b, 2019; Nassar et al., 2017; Schwandner et al., 2017; Matsunaga and Maksyutov, 2018; Miller et al., 2019; Labzovskii et al., 2019; Wu et al., 2020; Zheng et al., 2020a; Ye et al., 2020) and for other applications such as climate model assessments (e.g., Lauer et al., 2017; Gier et al., 2020) or data assimilation (e.g., Massart et al., 2016).

Here we use an ensemble of satellite retrievals of XCO_2 to determine whether COVID-19 related regional-scale (here ~2000^2 km^2) CO_2 emission reductions can be detected and quantified using the current space-based observing system. This is important in order to establish the capabilities of current satellites, which have been optimized to obtain information on natural carbon sources and sinks, but not to obtain information on anthropogenic emissions. Nevertheless, data from existing satellites have already been used to assess anthropogenic emissions (see publications cited above). These assessments and the assessment presented in this publication are relevant for future satellites focussing on anthropogenic emissions such as the planned European Copernicus Anthropogenic CO_2 Monitoring (CO2M) mission (e.g., ESA, 2019; Kuhlmann et al., 2019; Janssens-Maenhout et al., 2020), which is based on the CarbonSat concept (Bovensmann et al., 2010; Velazco et al., 2011; Buchwitz et al., 2013; Pillai et al., 2016; Broquet et al., 2018; Lespinas et al., 2020).

We focus on China because regional-scale COVID-19 related CO_2 emission reductions are expected to be largest there early in the pandemic (Le Quéré et al., 2020; Liu et al., 2020). Satellite data have been used to estimate China's CO_2 emissions during the COVID-19 pandemic as shown in Zheng et al., 2020b, but that study inferred CO_2 reductions from retrievals of nitrogen dioxide (NO_2) not using XCO_2. Estimates of emission reductions have also been derived from bottom-up statistical assessments of fossil fuel use and other economic indicators. According to Le Quéré et al., 2020, China's CO_2 emissions

decreased by 242 $MtCO_2$ (uncertainty range 108 – 394 $MtCO_2$) during January – April 2020. As China's annual CO_2 emissions

65 are approximately 10 $GtCO_2$/year (Friedlingstein et al., 2019), i.e., approximately 3.3 $GtCO_2$ in a 4-month period assuming constant emissions, the average relative (COVID-19 related) change during January – April 2020 is therefore approximately $7\% \pm 4\%$ (0.242/3.3 $\pm$ 0.14/3.3). This agrees reasonably well with the estimate reported in Liu et al., 2020, which is 9.3% for China during the first quarter of 2020 compared to the same period in 2019. Liu et al., 2020, also indicate some challenges in terms of interpreting CO_2 emission reductions as being caused by COVID-19, e.g., the fact that the first months of 2020 were

70 exceptionally warm across much of the northern hemisphere. CO_2 emissions associated with home heating may have therefore been somewhat lower than for the same period in 2019, even without the disruption in economic activities and energy production caused by COVID-19 and related lockdowns.

Sussmann and Rettinger, 2020, studied ground-based remote sensing XCO_2 retrievals of the Total Carbon Column Observing Network (TCCON) to find out whether related atmospheric concentration changes may be detected by the

75 TCCON and brought into agreement with bottom-up emission-reduction estimates. Our study is one of the first attempts to determine whether COVID-19 related regional-scale CO_2 emission reductions can be detected using existing space-based observations of XCO_2. Tohjima et al., 2020, inferred estimates of China's CO_2 emissions from modelled and observed ratios of CO_2 and methane (CH_4) surface concentrations at Hateruma Island, Japan. They report for China fossil fuel emission reductions of $32 \pm 12\%$ and $19 \pm 15\%$ for February and March 2020, respectively, which is about 10% higher compared to

80 the results shown in Le Quéré et al., 2020 (see Tab.1 of Tohjima et al., 2020). From model sensitivity simulations they conclude that even a 30% reduction of China's fossil fuel CO_2 emissions would only result in a 0.8 ppm XCO_2 reduction over China and that it therefore would be very challenging to detect any COVID-19 related signal with the existing remote sensing satellites GOSAT and OCO-2. Their conjecture has essentially been confirmed by Chevallier et al., 2020. They used XCO_2 from OCO-2 in combination with other data sets and the modelling of CO_2 emission plumes of localized CO_2 sources

85 to obtain estimates of CO_2 emissions focussing on several COVID-19 relevant regions such as China, Europe, India and the USA. They concluded that these places have not been well observed by the OCO-2 satellite because of frequent or persistent cloud conditions and they give recommendations for future carbon-monitoring systems. Zeng et al., 2020, used modelling, GOSAT XCO_2 and other data sets. They conclude that GOSAT is able to detect a short-term global mean XCO_2 anomaly decrease of 0.2-0.3 ppm after temporal averaging (e.g., monthly) but for East China they could not identify a statistically

90 robust COVID-19 related anomaly. Satellite-derived results related to this application are also provided in the internet (e.g., ESA-NASA-JAXA, 2020).

Regional-scale reductions of tropospheric NO_2 columns have been reported for China (e.g., Zhang et al., 2020; Bauwens et al., 2020), but for CO_2 such an assessment is more challenging because of small XCO_2 changes on top of a large background. For example, over extended anthropogenic source areas such as East China, the XCO_2 enhancement due to anthropogenic

95 emissions is typically only approximately 1 - 2 ppm (0.25% - 0.5% of 400 ppm) or even less (see, e.g., Schneising et al., 2008, 2013; Hakkarainen et al., 2016, 2019; Chevallier et al., 2020; Tohjima et al., 2020; and this study). A 10% emission

reduction would therefore only change the regional XCO_2 enhancement by 0.1 to 0.2 ppm. This is below the single measurement precision of current satellite XCO_2 data products (at footprint size, i.e., 10.5 km diameter for GOSAT (Kuze et al., 2016) and 1.3 x 2.3 km^2 for OCO-2 (O'Dell et al., 2018)), which is about 1.8 ppm (1-sigma) (e.g., Dils et al., 2014;

100   Kulawik et al., 2016; Buchwitz et al., 2015, 2017a; Reuter et al., 2020) for GOSAT and around 1 ppm for OCO-2 (Wunch et al., 2017; Reuter et al., 2019). In our study we focus on XCO_2 monthly averages. Averaging reduces the noise of the satellite retrievals (e.g., Kulawik et al., 2016) but also eliminates day-to-day XCO_2 variations (e.g., Agustí-Panareda et al., 2019), which cannot be interpreted using our simple analysis methods. The accuracy of the East China satellite XCO_2 retrievals averaged over monthly timescales is difficult to assess because of limited reference data. The validation of the satellite data

105   products is primarily based on comparisons with ground-based XCO_2 retrievals from the TCCON, a relatively sparse network with an uncertainty of about 0.4 ppm (Wunch et al., 2010).

The purpose of this study is to investigate - using satellite XCO_2 retrievals - if satellite-derived East China fossil fuel (FF) CO_2 emissions in 2020 (COVID-19 period) differ significantly compared to pre-COVID-19 periods. Ideally, we would like to know by how much emissions have been reduced due to COVID-19. This question, however, cannot be answered using only satellite

110   data because they do not contain any information on how much would have been emitted without COVID-19. Instead, we aim at answering the following question: Are satellite-derived East China FF CO_2 emissions early in the pandemic (here: January – May 2020) significantly lower compared to pre-COVID-19 periods?

To answer this question, we analyse relative differences of estimates of East China monthly FF emissions during different time periods. We focus on October to May periods and we refer to different periods via the year where a period ends, i.e., we call

115   the period October 2019 to May 2020 "year 2020 period" or simply "2020", the period October 2018 to May 2019 is called 2019, etc. Specifically, we compute and analyse differences of monthly emissions in the year 2020 period relative to previous year 2016 to 2019 periods, i.e., we use 4 periods for comparison with the year 2020 period. To focus on the COVID-19 aspect, we subtract for each period the October to December (OND) mean value and we refer to these time series as OND anomalies. These OND anomalies are time series at monthly resolution of relative emission difference between different periods relative

120   to OND. Negative OND anomalies during the COVID-19 period would then suggest (depending on uncertainty) that an emission reduction during the COVID-19 period has been detected.

The structure of our manuscript reflects this procedure: In the Data Section 2 we present the satellite and model input data used for this study. In the Methods Section 3 we present the analysis method, which consists of two main steps. The purpose of the first step is to isolate the East China FF emission signal from the XCO_2 satellite retrievals. This is done by subtracting

125   appropriate XCO_2 background values from the XCO_2 retrievals to obtain XCO_2 anomalies, ΔXCO_2. We use two methods to compute ΔXCO_2. We describe one method, the "DAM method", in detail in Sect. 3.1 and only shortly explain the second method ("TmS method") referring for details to Appendix A. In the second step (Sect. 3.2) we compute estimates of East China monthly FF CO_2 emissions from the XCO_2 anomalies. These emission estimates are then used to compute the OND

anomalies explained above. In Results Section 4 we present and discuss the results, i.e., the application of the described
130 methods to the satellite data. A summary and conclusions are given in Sect. 5.

2 Data

In this section, we present a short overview about the input data used for this study.

2.1 Satellite XCO_2 retrievals

This study uses four satellite XCO_2 Level 2 (L2) data products. An overview about these data sets is provided in Tab. 1. The
first product listed in Tab. 1 is the latest version of the bias-corrected OCO-2 XCO_2 product delivered to the Goddard Earth
Science Data and Information Services Center (GES DISC) by the OCO-2 team (ACOS v10r Lite). The other three satellite
XCO_2 datasets are different versions of the GOSAT XCO_2 product derived using retrieval algorithms developed by groups at
140 the University of Leicester, U.K. (UoL-FP v7.3), the SRON Netherlands Institute for Space Research (RemoTeC v2.3.8), and
the University of Bremen, Germany (FOCAL v1.0).

The XCO_2 estimates derived from OCO-2 (e.g., O'Dell et al., 2018) and GOSAT (e.g., Kuze et al., 2016) observations are
complementary because these two spacecraft use different sampling strategies. OCO-2 has been operating since September
2014. Its spectrometers collect about 85000 cloud-free XCO_2 soundings each day along a narrow (< 10 km) ground track as
145 it orbits the Earth 14.5 times each day from its sun synchronous 1:36 PM orbit. The OCO-2 soundings provide continuous
measurements with relatively high spatial resolution (1.3 x 2.3 km^2) along each track, but the individual ground tracks are
separated by almost 25° longitudes in any given day. This spacing is reduced to approximately 1.5° longitude after a 16-day
ground track repeat cycle. GOSAT has been returning 300 to 1000 cloud-free XCO_2 soundings each day since April 2009. Its
TANSO-FTS spectrometer collects soundings with 10.5 km diameter surface footprints, separated by approximately 250 km
150 along and across its ground track at it orbits from north to south across the sunlit hemisphere.

2.2 Model CO_2 data

We use data from NOAA's (National Oceanic and Atmospheric Administration) CO_2 assimilation system, CarbonTracker
(CT2019) (Jacobson et al., 2020; Peters et al., 2007) to define the relationship between XCO_2 anomalies and fossil fuel
emissions. CarbonTracker is a global atmospheric inverse model that assimilates atmospheric CO_2 measurements to produce
155 modelled fields of atmospheric CO_2 mole fractions by adjusting land biosphere and ocean CO_2 surface fluxes. An overview
about CT2019 set is provided in Tab. 2 including references and access information. In short, CarbonTracker has a
representation of atmospheric transport based on weather forecasts, and modules representing air-sea exchange of CO_2,
photosynthesis and respiration by the terrestrial biosphere, and release of CO_2 to the atmosphere by fires and combustion of
fossil fuels.

160

3. Methods

3.1 Methods to compute XCO₂ anomalies (ΔXCO₂)

Satellite XCO_2 retrievals contain information on anthropogenic CO_2 emissions (e.g., Schneising et al., 2013; Reuter et al.,

165 2014b, 2019; Nassar et al., 2017) but extracting this information requires appropriate data processing and analysis. For a strong (net) source region XCO_2 is typically higher compared to its surrounding area. Our method is based on computing and subtracting XCO_2 background values. The purpose of this background correction is to isolate the regional emission signal by removing large-scale spatial and day-to-day temporal XCO_2 variations, which cannot be dealt with in our simple data-driven method to estimate emissions.

170 XCO_2 varies temporally and spatially (e.g., Agustí-Panareda et al., 2019; Reuter et al., 2020; Gier et al., 2020), for example, due to quasi-regular uptake and release of CO_2 by the terrestrial biosphere, which results in a strong seasonal cycle, especially over northern mid and high latitudes. Compared to fluctuations originating from the interaction of the terrestrial biosphere and the atmosphere, the spatio-temporal XCO_2 variations due to anthropogenic fossil fuel (FF) CO_2 emissions are typically much smaller (e.g., 1 ppm compared to 10 ppm (Schneising et al., 2008, 2013, 2014; Agustí-Panareda et al.,

175 2019)).

A method used for background correction is the one described in Hakkarainen et al., 2019 (see also Hakkarainen et al., 2016, for a first publication of that method). We use two different methods for background correction. We refer to these methods as "Daily Anomalies via (latitude band) Medians" (DAM), which is essentially identical with the method described in Hakkarainen et al., 2019, and a second method called "Target minus Surrounding" (TmS).

180 Hakkarainen et al., 2019, applied their method to the OCO-2 Level 2 XCO_2 data product to filter out trends and seasonal variations in order to isolate CO_2 source/sink signals. For background correction, Hakkarainen et al., 2019, calculate daily medians for 10-degree latitude bands and linearly interpolate the resulting values to each OCO-2 data point. Instead of interpolation, we compute the median around each latitude ("running median") using a latitude band width of ±15 deg. We use a larger width compared to Hakkarainen et al., 2019, as we also apply our method to GOSAT data, which are much

185 sparser than OCO-2 data. Our investigations showed that the width of the latitude band is not critical. The band needs to be wide enough to contain a statistically significant sample, but narrow enough to resolve large latitudinal gradients in CO_2. We subtract the corresponding median from each single XCO_2 observation in the original Level 2 XCO_2 data product files to obtain a data set of XCO_2 anomalies, ΔXCO_2^{DAM}.

In order to verify that our results do not critically depend on the details of one method we also use the second TmS method.

190 Here we obtain the background by averaging XCO_2 in a region surrounding the target region (see Tab. 3 for the latitude and longitude corner coordinates of the target and its surrounding region).

We call these background corrected XCO_2 retrievals XCO_2 anomalies and satellite-derived maps and time series of these XCO_2 anomalies are presented and discussed in Sect. 4.1. These XCO_2 anomalies are then used to compute East China FF CO_2 emission estimates, CO_2^{FF}, as described in the following sub-section.

195

3.2 Computation of emission estimates (CO_2^{FF})

To determine whether satellite XCO_2 retrievals can provide information on relative changes of anthropogenic CO_2 emissions for the East China target region, we must establish a relationship between the XCO_2 anomalies (see Sect. 3.1) and the desired estimates of the target region fossil fuel (FF) emissions. To develop a method to convert the XCO_2 anomalies, ΔXCO_2, to FF

200   emission estimates, CO_2^{FF}, we use an existing model data set, the CarbonTracker CT2019 data set described in Sect. 2.2, which contains atmospheric CO_2 fields and corresponding CO_2 surface fluxes during 2015 – 2018.

Figure 1 shows CT2019 XCO_2 maps (left) and corresponding surface CO_2 flux maps (right) for selected days in the January to May 2018 period. The XCO_2 has been computed by vertically integrating the CT2019 CO_2 vertical profiles (weighted with the surface pressure normalized pressure change over each layer). The model data are sampled at local noon, which is close to

205   the overpass time of the satellite data sets used here. The spatio-temporal sampling of a specific satellite XCO_2 data product is not considered here, i.e., we use the CT2019 data set independent of any satellite data product apart for the sampling at local noon. As can be seen from Fig. 1, XCO_2 is clearly elevated over the East China target region (red rectangle) relative to its surrounding region on 15-January-2018 (Fig. 1(a)) and on 15-March-2018 (Fig. 1(c)). On 15-May-2018 (Fig. 1(e)) the target region and parts of the surrounding region contain large areas of lower than average XCO_2, a pattern which primarily results

210   from carbon uptake by vegetation during the growing season, which starts in eastern China around May each year. The CO_2 fluxes, which are shown on the right-hand side panels of Fig. 1, show similar spatial pattern as the XCO_2 maps but due to atmospheric transport and the long lifetime of atmospheric CO_2 there is no one-to-one correspondence between atmospheric XCO_2 and surface emissions. The CO_2 fluxes are the sum of several contributing fluxes including FF emissions, biogenic fluxes and other fluxes (fires, oceans).

215   Figure 2(a) shows time series obtained by applying the DAM method to CT2019 XCO_2 for the East China target region. The CT2019 data set not only contains atmospheric CO_2 concentrations but also its components due to fossil fuel (FF) emissions and biogenic (BIO) and other fluxes. From the CT2019 data set we computed total XCO_2 (TOT), and its FF and BIO components. From these components we subtracted the background using the DAM method and the corresponding monthly ΔXCO_2^{DAM} time series are shown in Fig. 2(a). As can be seen from Fig. 2(a), total ΔXCO_2^{DAM} (black line) is dominated by its

220   FF (red line) and BIO (green line) components (their sum, i.e., FF + BIO (grey line), is close to TOT (black line)). As can also be seen, FF emissions for East China (red line) are larger than the BIO fluxes (green line) at least during October to April. During May to September the BIO fluxes are negative due to uptake of atmospheric CO_2 by the terrestrial biosphere and their absolute value is on the same order or may even significantly exceed the FF emissions. As a consequence, total ΔXCO_2^{DAM}

(black line) gets negative. During these months, the total anomaly (black line) is closer to BIO (green line) than to FF (red
line).

The task for the satellite inversion is to obtain estimates of East China FF CO_2 emissions from the satellite-derived (total)
XCO_2 anomalies, ΔXCO_2^{DAM} (black line in Fig. 2(a)). To determine to what extent this is possible, we fitted CT2019
ΔXCO_2^{DAM} (i.e., the quantity that we can also obtain from satellites) to the East China CT2019 FF CO_2 emissions (which are
the known "true emissions" in this model data assessment exercise). The results are shown in Fig. 2(b) for October to May
periods. The estimated emissions (black crosses) have been obtained via a linear fit of ΔXCO_2^{DAM} to the CT2019 FF emissions
(red dots). The two parameters of the linear fit are also shown in 2(b): Scaling factor A (= 0.90) and offset B (= 7.41). As can
be seen, the estimated emissions agree reasonably well with the "true" emissions. The linear correlation coefficient R is 0.83
(see Fig. 2(c)) and the relative difference in terms of mean and standard deviation is 0.2% $\pm$ 5% (see Fig. 2(d)). However, for
individual months the error can be as large as 10%. From this we conclude that the (approximately 2-sigma) uncertainty of our
method is approximately 10%.

A similar figure but generated using the TmS method is shown in Appendix A as Fig. A1. As can be seen, the results shown
in Fig. A1 (b) to (d) are similar to the ones shown in Fig. 2 (b) to (d) but the linear correlation is slightly worse and the errors
are slightly larger. In contrast, the time series shown in panels (a) differ significantly. This is because of the different
background corrections used for the two methods. But despite these significant differences the quality of the derived emissions
is similar (the standard deviation of the monthly biases is 5.5% for TmS and 4.8% for DAM, see panels (d)). Nevertheless, the
DAM method gives slightly better results compared to the TmS method and this is also confirmed by applying both methods
to the satellite data (see Sect. 4). Therefore, the DAM method is our baseline method and we focus on results obtained with
the DAM method.

It is perhaps surprising that the offset (fit parameter B, see above) is so large (7.41 for DAM and 7.63 for TmS). Probably one
would assume that the XCO_2 anomalies ΔXCO_2 are directly proportional to the target region fossil fuel emissions, i.e., one
would assume that FF is (approximately) equal to a constant multiplied by ΔXCO_2 (no offset added) (for example, for FF = 8
$GtCO_2$/year and ΔXCO_2 = 2 ppm one would have expected that the conversion factor is 4 $GtCO_2$/year/ppm). In that case, as
we are only interested in relative changes in emissions, we would not need to know the exact value of the scaling factor.
However, when analysing the satellite data, we found that ΔXCO_2 is around 2 ppm for January but decreases in subsequent
months, nearly approaching zero in May (which is consistent with the CT2019 results shown in Fig. 2(a)). As anthropogenic
emissions are not expected to change that much within a few months (and zero emissions around May are not realistic at all)
we concluded that the simple proportionality assumption does not hold. To investigate this we used the CT2019 data set to test
and improve our method and the results are reported in this section. We applied our method to CT2019 XCO_2 (as shown in
Fig. 2) and compared the retrieved FF values with the ("true") CT2019 FF values. We found large differences, which could be
significantly reduced by adding an offset to the linear fit as discussed above. The reason for the large offset is the influence of

the biosphere. Around May the uptake of atmospheric CO_2 due to the biosphere is so large that ΔXCO_2 is close to zero - but the FF emissions are not - and the East China target regions is essentially "carbon neutral" or even a net sink (see also Fig. 1).

As explained, scaling factor A and offset B are obtained empirically via a linear fit using CT2019 data (Fig. 2(b)) and used for the conversion of the satellite XCO_2 anomalies during the entire time period January 2015 to May 2020 (as will be shown in Sect. 4). As can be seen from Fig. 2 (b) and (c), the retrieval biases are within $\pm 10\%$ during 2015-2018. We assume in our study that the same conversion is also appropriate for 2019 and 2020. However, it cannot be ruled out that 2019 or 2020 were significantly different compared to previous years with respect to aspects relevant for our study. To address this, we compare period October 2019 to May 2020 results with the corresponding results from previous October to December periods to find out to what extent the period of interest, i.e., October 2019 to May 2020, is significantly different taking into account the year-to-year variability, which we use to obtain uncertainty estimates.

The methods described in this section have been applied to convert satellite-derived target region XCO_2 anomalies, ΔXCO_2, into estimated target region FF CO_2 emissions, CO_2^{FF}. How this has been done using the DAM method for background correction is explained in the following Sect. 4, where we refer for the corresponding TmS method results to Appendix A.

4. Results and discussion

In this section, we present results obtained by applying the DAM method (see Methods Sect. 3.1) to the satellite data to obtain XCO_2 anomalies from which we derive FF emission estimates (see Methods Sect. 3.2).

4.1 Application of the DAM method to satellite XCO_2 retrievals

The DAM method has been applied to the OCO-2 and GOSAT satellite XCO_2 data products listed in Tab. 1. Figure 3 shows a global OCO-2 DAM XCO_2 anomaly map at $1^o \times 1^o$ resolution for the period 2015 – 2019. A similar map is shown in Hakkarainen et al., 2019 (see their Fig. 3, top panel). The degree of agreement confirms the finding reported in Sect. 3.1 that the generation of these anomaly maps does not critically depend on how exactly the median is computed and used to subtract "the background". Hakkarainen et al., 2019, discuss their OCO-2 derived maps in quite some detail also in terms of seasonal averages and comparisons with model simulations. They show that positive anomalies correspond to fossil fuel combustion over major industrial areas including China. Their seasonal maps (see their Fig. 4) show a strong positive anomaly over East China (similar as shown here in Fig. 3) except for the June-August (JJA) summer season, where the XCO_2 anomaly can be negative. This is consistent with the CT2019 results presented in Sect. 3.2.

A zoom into Fig. 3 is presented in Fig. 4, which shows more details for China and its surrounding area. As can be seen from Fig. 4, ΔXCO_2^{DAM} is positive especially in the region between Beijing, Wuhan and Hong Kong with highest values in the area between Beijing and Shanghai. This positive anomaly indicates that this region is a strong CO_2 source region as also

290   discussed in Hakkarainen et al., 2019. As already explained, there is no one-to-one correspondence (especially not for every grid cell) between local XCO_2 anomalies and local CO_2 emissions (or uptake) because the emitted CO_2 is transported and mixed in the atmosphere. Furthermore, the satellite data are typically sparse due to strict quality filtering to avoid potential XCO_2 biases, for example, due to the presence of clouds. Cloud contaminated ground scenes are identified to the extent possible via the corresponding retrieval algorithm (see references listed in Tab. 1) and flagged to be "bad" and are therefore

295   not used for this analysis. The sparseness of the satellite data set is obvious from Fig. 5, which shows OCO-2 DAM XCO_2 anomaly maps for February during the six years 2015 to 2020.

A key difference between the OCO-2 and the GOSAT data products is the different sampling of the target region, with GOSAT having much sparser coverage compared to OCO-2. This is illustrated in Fig. 6, which shows February to March 2020 averages of the OCO-2 XCO_2 data product (Fig. 6a) and the three GOSAT data products (Fig. 6b – 6d) at 1°x1°

300   resolution. The OCO-2 product shown in Fig. 6a is NASA's OCO-2 operational "Atmospheric CO_2 Observations from Space" (ACOS) algorithm version 10r bias corrected XCO_2 product (the so called Lite product), which is referred to in this publication via the product identifier (ID) CO2_OC2_ACOS. The three GOSAT XCO_2 products are (see details and references as given in Tab. 1): Fig. 6b: University of Leicester's GOSAT product (ID CO2_GOS_OCFP); Fig. 6c: SRON Netherlands Institute for Space Research GOSAT product (CO2_GOS_SRFP); Fig. 6d: University of Bremen's GOSAT

305   product (CO2_GOS_FOCA) as retrieved with the "Fast atmOspheric traCe gAs retrievaL" (FOCAL) retrieval algorithm initially developed for OCO-2 (Reuter et al., 2017a, 2017b). As can be seen from Fig. 6, the spatial sampling of the target region is different for each product as only quality-filtered (i.e., "good") data are shown and the quality filtering is algorithm specific (see references listed in Tab. 1).

Figure 6 also shows as red rectangle the East China target region as defined for this study (the geographical coordinates are

310   listed in Tab. 3). The fossil fuel (FF) CO_2 emissions of this target region are approximately 8 $GtCO_2$/year, i.e., the selected target region covers approximately 80% of the FF emissions of entire China, which are approximately 10 $GtCO_2$/year (Le Quéré et al., 2018; Friedlingstein et al., 2019). In the following section we present East China FF emission estimates as derived from the satellite XCO_2 anomalies during and before the COVID-19 period.

315

4.2 Emission estimates

Carbon dioxide fossil fuel emission estimates, CO_2^{FF}, have been derived from the XCO_2 anomalies, ΔXCO_2, computed for

320   each of the four satellite XCO_2 data products listed in Tab. 1. In this section the emission results are presented and discussed. We focus on results based on ΔXCO_2 derived with the DAM method and refer to Appendix A for results based on the TmS method.

4.2.1 Emission estimates from NASA's OCO-2 (version 10r) XCO₂

Figure 7 shows the results obtained by applying the DAM method to product CO2_OC2_ACOS (see Tab. 1) for the East China target region for the period January 2015 to May 2020 (the TmS version of this figure is shown as Fig. A2 in Appendix A). Figure 7(a) shows daily DAM XCO_2 anomalies as thin grey line and the corresponding monthly averages as red dots. The amplitude (approximately ±1 ppm) and time dependence (e.g., the minimum in the middle of each year) is similar as for CT2019 (Fig. 2(a) black line). To ensure that there are a sufficiently large number of observations per month, two criteria need to be fulfilled: There must be a minimum number of days per month (here: 5) and a minimum number observations per day (here: 30). The latter criterion is also relevant for the daily data shown in Fig. 7(a) (grey line). We also used other combinations of these two parameters (as shown below, e.g., Fig. 9).

Figure 7(b) shows monthly ΔXCO_2^{DAM} for different October to May periods and Fig. 7(c) shows the corresponding estimated FF emissions, $CO_2^{FF(DAM)}$. Figure 7(d) shows relative differences of the time series shown in Fig. 7(c). For example, the blue data are referred to as "(2020-2019)/2019" in Fig. 7(d), where 2019 refers to the blue data in Fig. 7(c), which corresponds to the period ending in May 2019. Shown are differences of year 2020 data (red in Fig. 7(c)) minus data from previous periods, i.e., Fig. 7(d) shows to what extent 2020 (strictly speaking the period 10.2019 – 5.2020, i.e., the period which ends in 2020) differs relative to previous October to May periods.

To find out if we can detect a difference between the COVID-19 period and pre-COVID-19 periods, we subtract from each time series shown in Fig. 7(d) the October to December (OND) mean value. The corresponding time series are shown in Fig. 7(e) and are referred to as "OND anomalies" in the following. As can be seen from Fig. 7(e), the OND anomalies vary within ±5%. Values before January scatter around zero as the mean value of OND anomalies is zero by definition during October to December. In January the values also scatter around zero. After January most values are negative indicating reduced emissions compared to pre-COVID-19 periods. This can be seen more clearly in Fig. 8, where the same data as in Fig. 7(e) are shown but in addition the ensemble mean (light blue thick lines and dots) and median (royal blue thick lines and dots) has been added including uncertainty estimates as computed from the standard deviation of the ensemble members.

Figures 7 and 8 have been generated with the requirement that for each day at least 30 observations need to be available in the target region and for each month at least 5 days fulfilling this 30 observations/day requirement. Figure 9 is similar to Fig. 8 except that also results for additional combinations have been added, i.e., other combinations of minimum number of observations per day and minimum number of days per month. As can be seen, the results depend somewhat on which combination of these parameters is used, but the ensemble median and its uncertainty (royal blue symbols and lines) is similar. The ensemble median values are similar and negative during February to May 2020. The large uncertainties (vertical lines; 1-sigma error estimates) reflect the scatter of the ensemble members. The errors bars (1-sigma) overlap with the zero (i.e., no reduction) line indicating that it cannot be claimed with confidence that a significant drop of the emissions during the COVID-19 period has been detected.

4.2.2 Emission estimates from GOSAT XCO$_2$ data products

The same analysis method as applied to NASA's OCO-2 data product (Sect. 4.2.1) has also been applied to the three
360 GOSAT XCO$_2$ data products listed in Tab. 1. The results are shown in Fig. 10 for product CO2_GOS_OCFP, in Fig. 11 for product CO2_GOS_SRFP, and in Fig. 12 for product CO2_GOS_FOCA. The month-to-month variations are larger for these GOSAT products compared to OCO-2 product (note the different scale of the y-axes compared to Fig. 9). This is because GOSAT products are much sparser compared to the OCO-2 product (as shown in Fig. 6) and because the single observation random error is larger for GOSAT compared to OCO-2. As can be seen from a comparison of the results obtained for the
365 three GOSAT products (Figs. 10 - 12) there are large difference among the results obtained from these products. For example, product CO2_GOS_OCFP (Fig. 10) suggests that the largest emission reduction is in April, in contrast to the other two products. The large spread of the GOSAT results means that no clear conclusions can be drawn concerning East China emission reductions during the COVID-19 period.

370 ### 4.2.3 Ensemble mean and uncertainty

An overview about the results obtained from all four satellite data products using the DAM method is shown in Fig. 13 (the corresponding TmS version of this figure is shown as Fig. A3 in Appendix A). The results obtained from the individual products (as shown in royal blue in Figs. 9 - 12) are shown here using reddish colours (the corresponding numerical values are listed in Tab. 4). Also shown in Fig. 13 is the mean of the ensemble members and its estimated uncertainty (in dark blue);
375 the corresponding numerical values are listed in the bottom row of Tab. 4. The ensemble mean suggests emission reductions by approximately 10% ± 10% in March and April 2020. However, as can also be seen, there are significant differences across the ensemble of satellite data products. For example, the analysis of the OCO-2 data suggests a much smaller emission reduction of only about 1-2%. Because of the large differences between the individual ensemble members it is concluded that the expected emission reduction cannot be reliably detected and accurately quantified with our method.
380

5 Summary and conclusions

We have analysed a small ensemble of satellite XCO$_2$ data products to investigate whether a regional-scale reduction of atmospheric CO$_2$ during the COVID-19 pandemic can be detected for East China. Specifically, we analysed four XCO$_2$ data
385 products from the satellites OCO-2 and GOSAT. For this purpose, we used a simple data-driven approach, which involves the computation of XCO$_2$ anomalies, ΔXCO$_2$, using a method called DAM (Daily Anomalies via (latitude band) Medians). This method, which is essentially identical with the method developed at Finnish Meteorological Institute (FMI, Hakkarainen et al., 2019), helps to isolate local or regional XCO$_2$ enhancements originating from anthropogenic CO$_2$ emissions from large-scale daily XCO$_2$ background variations (note however that the FMI method is not supposed to extract exclusively anthropogenic

390 emission contributions to XCO_2, see Hakkarainen et al., 2019). In addition to the DAM method we also used a second method for the computation of ΔXCO_2, which is referred to TmS (Target minus Surrounding). Using model and satellite data we found that the results obtained with the DAM method provide better results compared to the TmS method. Therefore, we focussed on DAM-based results but also report selected results obtained with the TmS method (reported separately in Appendix A). We analysed satellite data between January 2015 to May 2020 and compared year 2020 monthly XCO_2 anomalies with the

395 corresponding monthly XCO_2 anomalies from previous periods.

In order to link the satellite-derived XCO_2 anomalies to East China fossil fuel (FF) CO_2 emissions, we used output from NOAA's CO_2 assimilation system CarbonTracker (CT2019) covering the years 2015 to 2018. We focus on October to May periods to minimize the impact of the terrestrial biosphere. Using CT2019, we show that ΔXCO_2 can be converted to FF emission estimates, denoted CO_2^{FF}, via a linear transformation. The two coefficients slope and offset of this linear

400 transformation have been obtained empirically via a linear fit, i.e., we established a linear empirical equation to relate the two quantities ΔXCO_2 and CO_2^{FF}. We show using CT2019 that the retrieved emissions during October to May periods agree within 10% with the CT2019 East China FF emissions.

For the analysis of the satellite data we focus on the October 2019 to May 2020 period, which covers months during the COVID-19 pandemic but also pre-COVID-19 months. We compare results obtained during this period with earlier October to

405 May periods to find out to what extent year 2020 differs from previous years. Our analysis is limited to October to May periods because our simple data-driven analysis method cannot deal with the large and highly variable terrestrial biosphere CO_2 fluxes outside of this period. On the other hand this period is challenging for satellite retrievals because of the low sun angles especially during the winter months and cloudiness.

We applied our method to each of the four satellite XCO_2 data products to obtain monthly emission estimates, CO_2^{FF}, for East

410 China. We focus on changes relative to pre-COVID-19 periods. Our results show considerable month-to-month variability (especially for the GOSAT products) and significant differences across the ensemble of satellite data products analysed. The ensemble mean suggests emission reductions by approximately 10%±10% in March and April 2020. This estimate is dominated by the GOSAT ensemble members. Analysis of the OCO-2 product yields smaller values indicating a reduction of only about 1-2% with an uncertainty of approximately ±2%.

415 The large uncertainty, which is on the order of the derived reduction (i.e., 100%, 1-sigma), and the large spread of the results obtained for the individual ensemble members, indicates that it is challenging to reliably detect and to accurately quantify the emission reduction using the current generation of space based methods and the simple DAM-based analysis strategy adopted here.

These findings, which are consistent with other recent studies (e.g., Chevallier et al., 2020, Zeng et al., 2020), are not

420 unexpected. Regional XCO_2 enhancements due to fossil fuel emissions are typically only 1 to 2 ppm and even a 10% emission reduction would therefore only correspond to a reduction of the fossil fuel related regional XCO_2 enhancement by 0.1 to 0.2

ppm. XCO_2 variations as small as 0.2 ppm are below the estimated uncertainty of the single footprint satellite XCO_2 retrievals. The uncertainty of single observations, which is typically around 0.7 ppm (e.g., Buchwitz et al., 2017a; Reuter et al., 2020), has been obtained by comparisons with ground-based Total Carbon Column Observing Network (TCCON) XCO_2 retrievals, which have an uncertainty of 0.4 ppm (1-sigma, Wunch et al., 2010). In this study we focus on monthly averaged data because our analysis method cannot properly deal with day-to-day variability and because of the sparseness of the satellite data. Averaging results in reducing the random error but investigations have shown that random errors do not simply scale with the inverse of the square root of number of observations added due to (unknown) systematic errors and error correlations (Kulawik et al., 2016). Of course also other sources of uncertainty are relevant in this context, in particular time dependent atmospheric transport and varying biogenic CO_2 contributions (e.g., Houweling et al., 2015, and references given therein).

We conclude that inferring COVID-19 related information on regional-scale CO_2 emissions using current (quite sparse) satellite XCO_2 retrievals requires, if at all possible, a more sophisticated analysis method including the use of detailed *a priori* information and atmospheric transport modelling.

The extent to which COVID-19 related emission reductions can be resolved on smaller scales - such as power plants or cities (e.g., Nassar et al., 2017; Reuter et al., 2019; Zheng et al., 2020a; Wu et al., 2020) has not been investigated in this study. For this purpose, XCO_2 retrievals from NASA's OCO-3 mission are promising, especially because of its Snapshot Area Map (SAM) mode, which permits the mapping of XCO_2 over ~80 km by 80 km areas around localized anthropogenic CO_2 emission sources (see https://ocov3.jpl.nasa.gov/ (last access: 28-Aug-2020)). Even more complete coverage is planned for the Copernicus CO2M mission in the future (e.g., Janssens-Maenhout et al., 2020).

Acknowledgements

This study has been funded in parts by the European Space Agency (ESA) via projects ICOVAC (Impacts of COVID-19 lockdown measures on Air quality and Climate) and GHG-CCI+ (http://cci.esa.int/ghg, last access: 13-August-2020) and the University and the State of Bremen. We acknowledge financial support for the generation of several data sets used as input for this study: (i) European Commission via Copernicus Climate Change Service (C3S, https://climate.copernicus.eu/, last access: 22-July-2020) project C3S_312b_Lot2, (ii) the Japanese space agency JAXA (contract 19RT000692) and (iii) EUMETSAT (contract EUM/CO/19/4600002372/RL). H.Boe., Univ. Leicester, was funded as part of NERC's support of the National Centre for Earth Observation (NE/R016518/1).

We also acknowledge access to OCO-2 XCO_2 data product "OCO2_L2_Lite_FP 10r" obtained from NASA's Earthdata GES DISC website (https://disc.gsfc.nasa.gov/datasets?keywords=OCO-2%20v10r&page=1 (last access: 15-Aug-2020)).

We thank JAXA and the National Institute for Environmental Studies (NIES), Japan, for access to GOSAT Level 1 (L1) data and ESA for making the GOSAT L1 products available via the ESA Third Party Mission (TPM) archive.

We acknowledge CarbonTracker CT2019 results provided by NOAA ESRL, Boulder, Colorado, USA, from the website at http://carbontracker.noaa.gov (last access: 22-July-2020). We also acknowledge feedback from Andy Jacobson on an early draft of this manuscript.

Some of the work reported here was conducted by the Jet Propulsion Laboratory, California Institute of Technology under contract to NASA. Government sponsorship is acknowledged.

Author contributions

M.B. designed the study, performed the analysis and led the writing of this paper in close cooperation with M.R., S.N., B.F.A., H.B., J.P.B., O.S. K.B. and M.H. Input data and corresponding advice has been provided by M.R., S.N., A.D.N., H.Boe., L.W, J. L., I.A., C.W.O'D. and D.C. All authors contributed to significantly improve the manuscript.

Data availability. The key results of this study are listed in this manuscript in numerical form (Tab. 4). Access information for the satellite data used as input for this study is provided in Tab. 1. The CT2019 data are available from NOAA (see access information given in Tab. 2).

Competing financial interests

The authors declare no competing financial interests.

Appendix A

As explained in the main text, a second method has been applied to the CT2019 and the satellite data. This method is called

475   "Target minus Surrounding" (TmS) and differs from the DAM method in the approach to determine the XCO_2 background. Whereas the DAM method computes the (daily) background as the median of the XCO_2 values in latitude bands, the TmS background is computed from the XCO_2 values in an area surrounding the target region (the coordinates are listed in Tab. 3).

The TmS results are discussed in the main text. Here we only show three figures. Figure A1 is the same as Fig. 2 but using

480   the TmS method instead of the DAM method. Figure A2 is the TmS version of Fig. 7 and Fig. A3 is the TmS version of Fig. 13.

References

Agustí-Panareda, A., Diamantakis, M., Massart, S., Chevallier, F., Muñoz-Sabater, J., Barré, J., Curcoll, R., Engelen, R., Langerock, B., Law, R. M., Loh, Z., Morguí, J. A., Parrington, M., Peuch, V.-H., Ramonet, M., Roehl, C., Vermeulen, A. T., Warneke, T., and Wunch, D.: Modelling CO_2 weather – why horizontal resolution matters, Atmos. Chem. Phys., 19, 7347–7376, https://doi.org/10.5194/acp-19-7347-2019, 2019.

Basu, S., Guerlet, S., Butz, A., Houweling, S., Hasekamp, O., Aben, I., Krummel, P., Steele, P., Langenfelds, R., Torn, M., Biraud, S., Stephens, B., Andrews, A., and Worthy, D.: Global CO_2 fluxes estimated from GOSAT retrievals of total column CO_2, Atmos. Chem. Phys., 13, 8695–8717, doi:10.5194/acp-13-8695-2013, 2013.

Boesch, H., Anand, J., and Di Noia, A.: Product User Guide and Specification (PUGS) – ANNEX A for products CO2_GOS_OCFP, CH4_GOS_OCFP & CH4_GOS_OCPR (v7.2, 2009-2018), 3-Nov-2019, pp. 33, http://wdc.dlr.de/C3S_312b_Lot2/Documentation/GHG/PUGS/C3S_D312b_Lot2.3.2.3-v1.0_PUGS-GHG_ANNEX-A_v3.1.pdf (last access: 17-Aug-2020), 2019.

Bovensmann, H., Burrows, J. P., Buchwitz, M., Frerick, J., Noël, S., Rozanov, V. V., Chance, K. V., and Goede, A. H. P.: SCIAMACHY - Mission objectives and measurement modes, J. Atmos. Sci., 56 (2), 127-150, 1999.

Bovensmann, H., M. Buchwitz, J. P. Burrows, M. Reuter, T. Krings, K. Gerilowski, O. Schneising, J. Heymann, A. Tretner, and J. Erzinger, A remote sensing technique for global monitoring of power plant CO_2 emissions from space and related applications, Atmos. Meas. Tech., 3, 781-811, 2010.

Broquet, G., F.-M. Breon, E. Renault, M. Buchwitz, M. Reuter, H. Bovensmann, F. Chevallier, L. Wu, and P. Ciais, The potential of satellite spectro-imagery for monitoring CO_2 emissions from large cities, Atmos. Meas. Tech., 11, 681-708, https://doi.org/10.5194/amt-11-681-2018, 2018.

Buchwitz, M., Reuter, M., Bovensmann, H., Pillai, D., Heymann, J., Schneising, O., Rozanov, V., Krings, T., Burrows, J. P., Boesch, H., Gerbig, C., Meijer, Y., and Loescher, A.: Carbon Monitoring Satellite (CarbonSat): assessment of atmospheric CO_2 and CH_4 retrieval errors by error parameterization, Atmos. Meas. Tech., 6, 3477-3500, 2013.

Buchwitz, M., Reuter, M., Schneising, O., Boesch, H., Guerlet, S., Dils, B., Aben, I., Armante, R., Bergamaschi, P., Blumenstock, T., Bovensmann, H., Brunner, D., Buchmann, B., Burrows, J. P., Butz, A., Chédin, A., Chevallier, F., Crevoisier, C. D., Deutscher, N. M., Frankenberg, C., Hase, F., Hasekamp, O. P., Heymann, J., Kaminski, T., Laeng, A., Lichtenberg, G., De Mazière, M., Noël, S., Notholt, J., Orphal, J., Popp, C., Parker, R., Scholze, M., Sussmann, R., Stiller, G. P., Warneke, T., Zehner, C., Bril, A., Crisp, D., Griffith, D. W. T., Kuze, A., O'Dell, C., Oshchepkov, S., Sherlock, V., Suto, H., Wennberg, P., Wunch, D., Yokota, T., and Yoshida, Y.: The Greenhouse Gas Climate Change Initiative (GHG-

CCI): comparison and quality assessment of near-surface-sensitive satellite-derived CO_2 and CH_4 global data sets, Remote Sensing of Environment, 162, 344-362, doi:10.1016/j.rse.2013.04.024, 2015.

Buchwitz, M., Reuter, M., Schneising, O., Hewson, W., Detmers, R. G., Boesch, H., Hasekamp, O. P., Aben, I., Bovensmann, H., Burrows, J. P., Butz, A., Chevallier, F., Dils, B., Frankenberg, C., Heymann, J., Lichtenberg, G., De Maziere, M., Notholt, J., Parker, R., Warneke, T., Zehner, C., Griffith, D. W. T., Deutscher, N. M., Kuze, A., Suto, H., and Wunch, D.: Global satellite observations of column-averaged carbon dioxide and methane: The GHG-CCI XCO_2 and XCH_4 CRDP3 data set, Remote Sensing of Environment 203, 276-295, http://dx.doi.org/10.1016/j.rse.2016.12.027, 2017a.

Buchwitz, M., Schneising, O., Reuter, M., Heymann, J., Krautwurst, S., Bovensmann, H., Burrows, J. P., Boesch, H., Parker, R. J., Somkuti, P., Detmers, R. G., Hasekamp, O. P., Aben, I., Butz, A., Frankenberg, C., Turner, A. J., Satellite-derived methane hotspot emission estimates using a fast data-driven method, Atmos. Chem. Phys., 17, 5751-5774, doi:10.5194/acp-17-5751-2017, 2017b.

Buchwitz, M., Reuter, M., Schneising, O., Noel, S., Gier, B., Bovensmann, H., Burrows, J. P., Boesch, H., Anand, J., Parker, R. J., Somkuti, P., Detmers, R. G., Hasekamp, O. P., Aben, I., Butz, A., Kuze, A., Suto, H., Yoshida, Y., Crisp, D., and O'Dell, C.: Computation and analysis of atmospheric carbon dioxide annual mean growth rates from satellite observations during 2003-2016, Atmos. Chem. Phys., 18, 17355-17370, https://doi.org/10.5194/acp-18-17355-2018, 2018.

Burrows, J. P., Hölzle, E., Goede, A. P. H., Visser, H., and Fricke, W.: SCIAMACHY—Scanning Imaging Absorption Spectrometer for Atmospheric Chartography, Acta Astronaut., 35(7), 445–451, doi:10.1016/0094-5765(94)00278-t, 1995.

Butz, A., Guerlet, S., Hasekamp, O., Schepers, D., Galli, A., Aben, I., Frankenberg, C., Hartmann, J.-M., Tran, H., Kuze, A., Keppel-Aleks, G., Toon, G., Wunch, D., Wennberg, P., Deutscher, N., Griffith, D., Macatangay, R., Messerschmidt, J., Notholt, J., and Warneke, T.: Toward accurate CO_2 and CH_4 observations from GOSAT, Geophys. Res. Lett., doi:10.1029/2011GL047888, 2011.

Chevallier, F.: On the parallelization of atmospheric inversions of CO_2 surface fluxes within a variational framework, Geosci. Model. Dev., 6, 783-790, doi:10.5194/gmd-6-783-2013, 2013.

Chevallier, F., Palmer, P. I., Feng, L., Boesch, H., O'Dell, C. W., and Bousquet, P.: Towards robust and consistent regional CO_2 flux estimates from in situ and space-borne measurements of atmospheric CO_2, Geophys. Res. Lett., 41, 1065–1070, doi:10.1002/2013GL058772, 2014.

Chevallier, F.: On the statistical optimality of CO_2 atmospheric inversions assimilating CO_2 column retrievals, Atmos. Chem. Phys., 15, 11133–11145, https://doi.org/10.5194/acp-15-11133-2015, 2015.

Chevallier, F., Zheng, B., Broquet, G., Ciais, P., Liu, Z., Davis, S. J., Deng, Z., Wang, Y., Bréon, F.-M., and O'Dell, C. W.: Local anomalies in the column-averaged dry air mole fractions of carbon dioxide across the globe during the first months of the coronavirus recession. Geophysical Research Letters, 47, e2020GL090244. https://doi.org/10.1029/2020GL090244, 2020.

545   Ciais, P., Dolman, A. J., Bombelli, A., Duren, R., Peregon, A., Rayner, P. J., Miller, C., Gobron, N., Kinderman, G., Marland, G., Gruber, N., Chevallier, F., Andres, R. J., Balsamo, G., Bopp, L., Bréon, F.-M., Broquet, G., Dargaville, R., Battin, T. J., Borges, A., Bovensmann, H., Buchwitz, M., Butler, J., Canadell, J. G., Cook, R. B., DeFries, R., Engelen, R., Gurney, K. R., Heinze, C., Heimann, M., Held, A., Henry, M., Law, B., Luyssaert, S., Miller, J., Moriyama, T., Moulin, C., Myneni, R. B., Nussli, C., Obersteiner, M., Ojima, D., Pan, Y., Paris, J.-D., Piao, S. L., Poulter, B., Plummer, S., Quegan, S.,

550   Raymond, P., Reichstein, M., Rivier, L., Sabine, C., Schimel, D., Tarasova, O., Valentini, R., Wang, R., van der Werf, G., Wickland, D., Williams, M., and Zehner, C.: Current systematic carbon-cycle observations and the need for implementing a policy-relevant carbon observing system, Biogeosciences, 11, 3547–3602, https://doi.org/10.5194/bg-11-3547-2014, 2014.

Ciais, P., Crisp, D., Denier van der Gon, H., Engelen, R., Janssens-Maenhout, G., Heimann, H., Rayner, P., and Scholze, M.: Towards a European Operational Observing System to Monitor Fossil CO_2 emissions, Final Report from the expert group,

555   European Comission, October 2015, pp. 68, https://edgar.jrc.ec.europa.eu/news_docs/CO2_report_22-10-2015.pdf (last access: 26-Aug-2020), 2015.

Cogan, A. J., Boesch, H., Parker, R. J., Feng, L., Palmer, P. I., Blavier, J.-F. L., Deutscher, N. M., Macatangay, R., Notholt, J., Roehl, C., Warneke, T., and Wunsch, D.: Atmospheric carbon dioxide retrieved from the Greenhouse gases Observing SATellite (GOSAT): Comparison with ground-based TCCON observations and GEOS-Chem model calculations, J.

560   Geophys. Res., 117, D21301, doi:10.1029/2012JD018087, 2012.

Crisp, D., Atlas, R. M., Bréon, F.-M., Brown, L. R., Burrows, J. P., Ciais, P., Connor, B. J., Doney, S. C., Fung, I. Y., Jacob, D. J., Miller, C. E., O'Brien, D., Pawson, S., Randerson, J. T., Rayner, P., Salawitch, R. S., Sander, S. P., Sen, B., Stephens, G. L., Tans, P. P., Toon, G. C.,Wennberg, P. O.,Wofsy, S. C., Yung, Y. L., Kuang, Z., Chudasama, B., Sprague, G.,Weiss, P., Pollock, R., Kenyon, D., and Schroll, S.: The Orbiting Carbon Observatory (OCO) mission, Advances in Space Research,

565   34, 700–709, 2004.

Crisp, D., Meijer, Y., Munro, R., Bowman, K., Chatterjee, A., Baker, D., Chevallier, F., Nassar, R., Palmer, P. I., Agusti-Panareda, A., Al-Saadi, J., Ariel, Y., Basu, S., Bergamaschi, P., Boesch, H., Bousquet, P., Bovensmann, H., Bréon, F.-M., Brunner, D., Buchwitz, M., Buisson, F., Burrows, J. P., Butz, A., Ciais, P., Clerbaux, C., Counet, P., Crevoisier, C., Crowell, S., DeCola, P. L., Deniel, C., Dowell, M., Eckman, R., Edwards, D., Ehret, G., Eldering, A., Engelen, R., Fisher, B.,

570   Germain, S., Hakkarainen, J., Hilsenrath, E., Holmlund, K., Houweling, S., Hu, H., Jacob, D., Janssens-Maenhout, G., Jones, D., Jouglet, D., Kataoka, F., Kiel, M., Kulawik, S. S., Kuze, A., Lachance, R. L., Lang, R., Landgraf , J., Liu, J., Liu, Y., Maksyutov, S., Matsunaga, T., McKeever, J., Moore, B., Nakajima, M., Natraj, V., Nelson, R. R., Niwa, Y., Oda, T., O'Dell, C. W., Ott, L., Patra, P., Pawson, S., Payne, V., Pinty, B., Polavarapu, S. M., Retscher, R., Rosenberg, R., Schuh, A., Schwandner, F. M., Shiomi, K., Su, W., Tamminen, J., Taylor, T. E., Veefkind, P., Veihelmann, B., Wofsy, S., Worden, J.,

575   Wunch, D., Yang, D., Zhang, P., and Zehner, C.: A CONSTELLATION ARCHITECTURE FOR MONITORING CARBON DIOXIDE AND METHANE FROM SPACE, Prepared by the CEOS Atmospheric Composition Virtual

Constellation Greenhouse Gas Team, Committee on Earth Observation Satellites, Version 1.0, 8 October 2018, pp. 173, http://ceos.org/document_management/Meetings/Plenary/32/documents/CEOS_AC-VC_White_Paper_Version_1_20181009.pdf (last access: 26-Aug-2020), 2018.

580 Eldering, A., Wennberg, P. O., Crisp, D., Schimel, D. S., Gunson, M. R., Chatterjee, A., Liu, J., Schwandner, F. M., Sun, Y., O'Dell, C. W., Frankenberg, C., Taylor, T., Fisher, B., Osterman, G. B., Wunch, D., Hakkarainen, J., Tamminen, J., and 305 Weir, B.: The Orbiting Carbon Observatory-2 early science investigations of regional carbon dioxide fluxes, Science, 358, eaam5745, doi: 10.1126/science.aam5745, 2017.

ESA, 2019: ESA, European Space Agency, Copernicus CO_2 Monitoring Mission Requirements Document, version 2.0 of
585 27/09/19, ESA Earth and Mission Science Division document ref. EOP-SM/3088/YM-ym, https://esamultimedia.esa.int/docs/EarthObservation/CO2M_MRD_v2.0_Issued20190927.pdf (last access: 15-July-2020), pp. 82, 2019.

ESA-NASA-JAXA, 2020: ESA, NASA and JAXA COVID-10 Dashboard (see: https://www.nasa.gov/coronavirus, https://www.nasa.gov/press-release/nasa-partner-space-agencies-amass-global-view-of-covid-19-impacts and/or
590 https://www.esa.int/ESA_Multimedia/Images/2020/06/COVID-19_Earth_Observation_Dashboard2, last access: 15-July-2020).

Dils, B. Buchwitz, M., Reuter, M., Schneising, O., Boesch, H. , Parker, R., Guerlet, S., Aben, I., Blumenstock, T., Burrows, J. P., Butz, A., Deutscher, N. M., Frankenberg, C., Hase, F., Hasekamp, O. P., Heymann, J., De Maziere, M., Notholt, J., Sussmann, R., Warneke, T., Griffith, D., Sherlock, V., and Wunch, D.: The Greenhouse Gas Climate Change Initiative
595 (GHG-CCI): comparative validation of GHG-CCI SCIAMACHY/ENVISAT and TANSO-FTS/GOSAT CO_2 and CH_4 retrieval algorithm products with measurements from the TCCON, Atmos. Meas. Tech., 7, 1723-1744, 2014.

Friedlingstein, P., Jones, M. W., O'Sullivan, M., Andrew, R. M., Hauck, J., Peters, G. P., Peters, W., Pongratz, J., Sitch, S., Le Quéré, C., Bakker, D. C. E., Canadell, J. G., Ciais, P., Jackson, R. B., Anthoni, P., Barbero, L., Bastos, A., Bastrikov, V., Becker, M., Bopp, L., Buitenhuis, E., Chandra, N., Chevallier, F., Chini, L. P., Currie, K. I., Feely, R. A., Gehlen, M.,
600 Gilfillan, D., Gkritzalis, T., Goll, D. S., Gruber, N., Gutekunst, S., Harris, I., Haverd, V., Houghton, R. A., Hurtt, G., Ilyina, T., Jain, A. K., Joetzjer, E., Kaplan, J. O., Kato, E., Klein Goldewijk, K., Korsbakken, J. I., Landschützer, P., Lauvset, S. K., Lefèvre, N., Lenton, A., Lienert, S., Lombardozzi, D., Marland, G., McGuire, P. C., Melton, J. R., Metzl, N., Munro, D. R., Nabel, J. E. M. S., Nakaoka, S. I., Neill, C., Omar, A. M., Ono, T., Peregon, A., Pierrot, D., Poulter, B., Rehder, G., Resplandy, L., Robertson, E., Rödenbeck, C., Séférian, R., Schwinger, J., Smith, N., Tans, P. P., Tian, H., Tilbrook, B.,
605 Tubiello, F. N., van der Werf, G. R., Wiltshire, A. J., and Zaehle, S.: Global Carbon Budget 2019, Earth Syst. Sci. Data, 11, 1783-1838, doi: 10.5194/essd-11-1783-2019, 2019.

Gier, B. K., Buchwitz, M., Reuter, M., Cox, P. M., Friedlingstein, P., and Eyring, V.: Spatially resolved evaluation of Earth system models with satellite column-averaged CO2, Biogeosciences, 17, 6115-6144, https://doi.org/10.5194/bg-17-6115-2020, 2020.

610 Hakkarainen, J., Ialongo, I., and Tamminen, J.: Direct space-based observations of anthropogenic CO_2 emission areas from OCO-2, Geophys. Res. Lett., 43, 11,400–11,406, doi:10.1002/2016GL070885, 2016.

Hakkarainen, J., Ialongo, I., Maksyutov, S., and Crisp, D.: Analysis of Four Years of Global XCO2 Anomalies as Seen by Orbiting Carbon Observatory-2, Remote Sensing, 11, 850, doi:10.3390/rs11070850, pp. 20, 2019.

Houweling, S., Baker, D., Basu, S., Boesch, H., Butz, A., Chevallier, F., Deng, F., Dlugokencky, E. J., Feng, L., Ganshin,
615 A., Hasekamp, O., Jones, D., Maksyutov, S., Marshall, J., Oda, T., O'Dell, C. W., Oshchepkov, S., Palmer, P. I., Peylin, P., Poussi, Z., Reum, F., Takagi, H., Yoshida, Y., and Zhuralev, R.: An intercomparison of inverse models for estimating sources and sinks of CO_2 using GOSAT measurements, J. Geophys. Res. Atmos., 120, 5253–5266, doi:10.1002/2014JD022962, 2015.

IPCC: Climate Change 2013: The Physical Science Basis, Working Group I Contribution to the Fifth Assessment Report of
620 the Intergovernmental Report on Climate Change, http://www.ipcc.ch/report/ar5/wg1/ (last access: 21-February-2019), Cambridge University Press, 2013.

Jacobson, A. R., Schuldt, K. N., Miller, J. B., Oda, T., Tans, P., Andrews, A., Mund, J., Ott, L., Collatz, G. J., Aalto, T., Afshar, S., Aikin, K., Aoki, S., Apadula, F., Baier, B., Bergamaschi, P., Beyersdorf, A., Biraud, S. C., Bollenbacher, A., Bowling, D., Brailsford, G., Abshire, J. B., Chen, G., Chen, H., Chmura, L., Colomb, A., Conil, S., Cox, A., Cristofanelli, P.,
625 Cuevas, E., Curcoll, R., Sloop, C. D., Davis, K., Wekker, S. D., Delmotte, M., DiGangi, J. P., Dlugokencky, E., Ehleringer, J., Elkins, J. W., Emmenegger, L., Fischer, M. L., Forster, G., Frumau, A., Galkowski, M., Gatti, L. V., Gloor, E., Griffis, T., Hammer, S., Haszpra, L., Hatakka, J., Heliasz, M., Hensen, A., Hermanssen, O., Hintsa, E., Holst, J., Jaffe, D., Karion, A., Kawa, S. R., Keeling, R., Keronen, P., Kolari, P., Kominkova, K., Kort, E., Krummel, P., Kubistin, D., Labuschagne, C., Langenfelds, R., Laurent, O., Laurila, T., Lauvaux, T., Law, B., Lee, J., Lehner, I., Leuenberger, M., Levin, I., Levula, J.,
630 Lin, J., Lindauer, M., Loh, Z., Lopez, M., Lund Myhre, C., Machida, T., Mammarella, I., Manca, G., Manning, A., Manning, A., Marek, M. V., Marklund, P., Martin, M. Y., Matsueda, H., McKain, K., Meijer, H., Meinhardt, F., Miles, N., Miller, C. E., Mölder, M., Montzka, S., Moore, F., Morgui, J.-A., Morimoto, S., Munger, B., Necki, J., Newman, S., Nichol, S., Niwa, Y., O'Doherty, S., Ottosson-Löfvenius, M., Paplawsky, B., Peischl, J., Peltola, O., Pichon, J.-M., Piper, S., Plass-Dölmer, C., Ramonet, M., Reyes-Sanchez, E., Richardson, S., Riris, H., Ryerson, T., Saito, K., Sargent, M., Sasakawa, M., Sawa, Y.,
635 Say, D., Scheeren, B., Schmidt, M., Schmidt, A., Schumacher, M., Shepson, P., Shook, M., Stanley, K., Steinbacher, M., Stephens, B., Sweeney, C., Thoning, K., Torn, M., Turnbull, J., Tørseth, K., Bulk, P. V. D., Laan-Luijkx, I. T. V. D., Dinther, D. V., Vermeulen, A., Viner, B., Vitkova, G., Walker, S., Weyrauch, D., Wofsy, S., Worthy, D., Young, D., and Zimnoch, M.: CarbonTracker CT2019, DOI: 10.25925/39m3-6069, 2020.

Janssens-Maenhout, G., Pinty, B., Dowell, M., Zunker, H., Andersson, E., Balsamo, G., Bezy, J.-L., Brunhes, T., Boesch, H.,
640   Bojkov, B., Brunner, D., Buchwitz, M., Crisp, D., Ciais, P., Counet, P., Dee, D., Denier van der Gon, H., Dolman, H.,
Drinkwater, M., Dubovik, O., Engelen, R., Fehr, T., Fernandez, V., Heimann, M., Holmlund, K., Houweling, S., Husband,
R., Juvyns, O., Kentarchos, A., Landgraf, J., Lang, R., Loescher, A., Marshall, J., Meijer, Y., Nakajima, M., Palmer, P. I.,
Peylin, P., Rayner, P., Scholze, M., Sierk, B., Tamminen, J., and Veefkind P.: Towards an operational anthropogenic CO_2
emissions monitoring and verification support capacity, Bulletin of the American Meteorological Society (BAMS),
645   10.1175/BAMS-D-19-0017.1, https://doi.org/10.1175/BAMS-D-19-0017.1, Published Online: 10 February 2020, 2020.

Kaminski, T., Scholze, M., Voßbeck, M., Knorr, W., Buchwitz, M, and Reuter, M.: Constraining a terrestrial biosphere
model with remotely sensed atmospheric carbon dioxide, Remote Sensing of Environment 203, 109-124, 2017.

Kiel, M., O'Dell, C. W., Fisher, B., Eldering, A., Nassar, R., MacDonald, C. G., and Wennberg, P. O.: How bias correction
goes wrong: measurement of XCO_2 affected by erroneous surface pressure estimates, Atmos. Meas. Tech., 12, 2241–2259,
650   https://doi.org/10.5194/amt-12-2241-2019, 2019.

Kuhlmann, G., Broquet, G., Marshall, J., Clément, V., Löscher, A., Meijer, Y., and Brunner, D.: Detectability of CO_2

emission plumes of cities and power plants with the Copernicus Anthropogenic CO_2 Monitoring (CO2M) mission, Atmos.

Meas. Tech., 12, 6695-6719, doi: 10.5194/amt-12-6695-2019, 2019.

Kulawik, S., Wunch, D., O'Dell, C., Frankenberg, C., Reuter, M., Oda, T., Chevallier, F., Sherlock, V., Buchwitz, M.,
655   Osterman, G., Miller, C. E., Wennberg, P. O., Griffith, D., Morino, I., Dubey, M. K., Deutscher, N. M., Notholt, J., Hase, F.,
Warneke, T., Sussmann, R., Robinson, J., Strong, K., Schneider, M., De Maziere, M., Shiomi, K., Feist, D. G., Iraci, L. T.,
Wolf, J.: Consistent evaluation of ACOS-GOSAT, BESD-SCIAMACHY, CarbonTracker, and MACC through comparisons
to TCCON, Atmos. Meas. Tech., 9, 683-709, doi:10.5194/amt-9-683-2016, 2016.

Kuze, A., Suto, H., Shiomi, K., Kawakami, S., Tanaka, M., Ueda, Y., Deguchi, A., Yoshida, J., Yamamoto, Y., Kataoka, F.,
660   Taylor, T. E., and Buijs, H. L.: Update on GOSAT TANSO-FTS performance, operations, and data products after more than
6 years in space, Atmos. Meas. Tech., 9, 2445-2461, doi:10.5194/amt-9-2445-2016, 2016.

Labzovskii, L. D., Jeong, S.-J., and Parazoo, N. C.: Working towards confident spaceborne monitoring of carbon emissions
from cities using Orbiting Carbon Observatory-2, Remote Sensing of Environment, 233, 111359, doi:
10.1016/j.rse.2019.111359, 2019.

665   Lauer, A., Eyring, V., Righi, M., Buchwitz, M., Defourny, P., Evaldsson, M., Friedlingstein, P., de Jeu, R., de Leeuw, G.,
Loew, A., Merchant, C. J., Müller, B., Popp, T., Reuter, M., Sandven, S., Senftleben, D., Stengel, M., Van Roozendael, M.,
Wenzel, S., and Willén, U.: Benchmarking CMIP5 models with a subset of ESA CCI Phase 2 data using the ESMValTool,
Remote Sensing of Environment, 203, 9-39, http://dx.doi.org/10.1016/j.rse.2017.01.007, 2017.

Lespinas, F., Wang, Y., Broquet, G., Breon, F.-M., Buchwitz, M., Reuter, M., Meijer, Y., Loescher, A., Janssens-Maenhout,
670   G., Zheng, B., and Ciais, P.: The potential of a constellation of low earth orbit satellite imagers to monitor worldwide fossil fuel CO2 emissions from large cities and point sources. Carbon Balance Manage 15, 18, pp. 12, https://doi.org/10.1186/s13021-020-00153-4 (last access: 1-Feb-2021), 2020.

Le Quéré, C., Andrew, R. M., Friedlingstein, P., Sitch, S., Pongratz, J., Manning, A. C., Korsbakken, J. I., Peters, G. P. Canadell, J. G., Jackson, R. B., Boden, T. A., Tans, P. P., Andrews, O. D., Arora, V. K., Bakker, D. D. E, Barbero, L.,
675   Becker, M., Betts, R. A., Bopp, L., Chevallier, F., Chini, L. P., Ciais, P., Cosca, C. E., Cross, J., Currie, K., Gasser, T., Harris, I., Hauck, J., Haverd, V., Houghton, R. A., Hunt, C. W., Hurtt, G., Ilyina, T., Jain, A. K., Kato, E., Kautz, M., Keeling, R. F., Goldewijk, K. K., Körtzinger, A., Landschützer, P., Lefèvre, N., Lenton, A., Lienert, S., Lima, I., Lombardozzi, D., Metzl, N., Millero, F., Monteiro, P. M. S., Munro, D. R., Nabel, J. E. M. S., Nakaoka, S., Nojiri, Y., Padín, X. A., Peregon, A., Pfeil, B., Pierrot, D., Poulter, B., Rehder, G., Reimer, J., Rödenbeck, C., Schwinger, J., Séférian, R.,
680   Skjelvan, I., Stocker, B. D., Tian, H., Tilbrook, B., van der Laan-Luijkx, I. T., van der Werf, G. R., van Heuven, S., Viovy, N., Vuichard, N., Walker, A. P., Watson, A. J., Wiltshire, A. J., Zaehle, S., and Zhu, D.: Global Carbon Budget 2017, Earth System Science Data, 10, 405-448, DOI: 10.5194/essd-10-405-2018, 2018.

Le Quéré, C., Jackson, R. B., Jones, M. W., Smith, A. J. P., Abernethy, S., Andrew, R. M., De-Gol, A. J., Willis, D. R., Shan, Y., Canadell, J. G., Friedlingstein, P., Creutzig, G. and Peters, G. P.: Temporary reduction in daily global CO_2
685   emissions during the COVID-19 forced confinement. *Nat. Clim. Chang.* **10,** 647–653, https://doi.org/10.1038/s41558-020-0797-x (last access: 15-July-2020), 2020.

Liu, J., Bowman, K. W., Schimel, D. S., Parazoo, N. C., Jiang, Z., Lee, M., Bloom, A. A., Wunch, D., Frankenberg, C., Sun, Y., O'Dell, C. W., Gurney, K. R., Menemenlis, D., Gierach, M., Crisp, D., and Eldering, A.: Contrasting carbon cycle responses of the tropical continents to the 2015–2016 El Niño, Science, 358, eaam5690, pp. 7, 2017.

690   Liu, Z., Ciais, P., Deng, Z., Lei, R., Davis, S. J., Feng, S., Zheng, B., Cui, D., Dou, X., He, P., Zhu, B., Lu, C., Ke, P., Sun, T., Wang, Y., Yue, X., Wang, Y., Lei, Y., Zhou, H., Cai, Z., Wu, Y., Guo, R., Han, T., Xue, J., Boucher, O., Boucher, E., Chevallier, F., Wei, Y., Zhong, H., Kang, C., Zhang, N., Chen, B., Xi, F., Marie, F., Zhang, Q., Guan, D., Gong, P., Kammen, D. M., He, K., and Schellnhuber, H. J.: Near-real-time-data captured record decline in global CO_2 emissions due to COVID-19, https://arxiv.org/ftp/arxiv/papers/2004/2004.13614.pdf (last access: 5-Jan-2021), pp. 45, 2020.

695   Massart, S., Agusti-Panareda, A., Heymann, J., Buchwitz, M., Chevallier, F., Reuter, M., Hilker, M., Burrows, J. P., Deutscher, N. M., Feist, D. G., Hase, F., Sussmann, R., Desmet, F., Dubey, M. K., Griffith, D. W. T., Kivi, R., Petri, C., Schneider, M., and Velazco, V. A.: Ability of the 4-D-Var analysis of the GOSAT BESD XCO_2 retrievals to characterize atmospheric CO_2 at large and synoptic scales, Atmos. Chem. Phys., 16, 1653-1671, doi:10.5194/acp-16-1653-2016, 2016.

Matsunaga, T., and Maksyutov, S. (eds.): A Guidebook on the Use of Satellite Greenhouse Gases Observation Data to
700   Evaluate and Improve Greenhouse Gas Emission Inventories, Satellite Observation Center, National Institute for

Environmental Studies, Japan, 1st Edition, March 2018, pp. 137,
https://www.nies.go.jp/soc/doc/GHG_Satellite_Guidebook_1st_12d.pdf (last access: 26-Aug-2020), 2018.

Miller, S. M., Michalak, A. M., Detmers, R. G., Hasekamp, O. P., Bruhwiler, L. M. P., and Schwietzke, S.: China's coal mine methane regulations have not curbed growing emissions, Nature Communications, volume 10, article number: 303, 2019.

Miller, S. M. and Michalak, A. M.: The impact of improved satellite retrievals on estimates of biospheric carbon balance, Atmos. Chem. Phys., 20, 323–331, https://doi.org/10.5194/acp-20-323-2020, 2020.

Nassar, R., Hill, T. G., McLinden, C. A., Wunch, D., Jones, D. B. A., and Crisp, D.: Quantifying CO_2 emissions from individual power plants from space. Geophysical Research Letters, 44, 10,045– 10,053. https://doi.org/10.1002/2017GL074702, 2017.

Noël, S., Reuter, M., Buchwitz, M., Borchardt, J., Hilker, M., Bovensmann, H., Burrows, J. P., Di Noia, A., Suto, H., Yoshida, Y., Buschmann, M., Deutscher, N. M., Feist, D. G., Griffith, D. W. T., Hase, F., Kivi, R., Morino, I., Notholt, J., Ohyama, H., Petri, C., Podolske, J. R., Pollard, D. F., Sha, M. K., Shiomi, K., Sussmann, R., Te, Y., Velazco, V. A., and Warneke, T.: XCO_2 retrieval for GOSAT and GOSAT-2 based on the FOCAL algorithm, Atmos. Meas. Tech. Discuss., https://doi.org/10.5194/amt-2020-453, in review, 2020.

O'Dell, C. W., Connor, B., Bösch, H., O'Brien, D., Frankenberg, C., Castano, R., Christi, M., Eldering, D., Fisher, B., Gunson, M., McDuffie, J., Miller, C. E., Natraj, V., Oyafuso, F., Polonsky, I., Smyth, M., Taylor, T., Toon, G. C.,Wennberg, P. O., andWunch, D.: The ACOS CO_2 retrieval algorithm – Part 1: The ACOS CO_2 retrieval algorithm – Part 1: Description and validation against synthetic observations, Atmos. Meas. Tech., 5, 99–121, doi:10.5194/amt-5-99-2012, 2012.

O'Dell, C. W., Eldering, A., Wennberg, P. O., Crisp, D., Gunson, M. R., Fisher, B., Frankenberg, C., Kiel, M., Lindqvist, H., Mandrake, L., Merrelli, A., Natraj, V., Nelson, R. R., Osterman, G. B., Payne, V. H., Taylor, T. R., Wunch, D., Drouin, B. J., Oyafuso, F., Chang, A., McDuffie, J., Smyth, M., Baker, D. F., Basu, S., Chevallier, F., Crowell, S. M. R., Feng, L., Palmer, P. I., Dubey, M., García, O. E., 15 Griffith, D. W. T., Hase, F., Iraci, L. T., Kivi, R., Morino, I., Notholt, J., Ohyama, H., Petri, C., Roehl, C. M., Sha, M. K., Strong, K.,Sussmann, R., Te, Y., Uchino, O., and Velazco, V. A.: Improved Retrievals of Carbon Dioxide from the Orbiting Carbon Observatory-2 with the version 8 ACOS algorithm, Atmos. Meas. Tech., 11, 6539-6576, https://doi.org/10.5194/amt-11-6539-2018, 2018.

Osterman, G., O'Dell, C., Eldering A., Fisher, B., Crisp, D., Cheng, C., Frankenberg, C., Lambert, A., Gunson, M., Mandrake, L., Wunch, D.: Orbiting Carbon Observatory-2 & 3 (OCO-2 & OCO-3) Data Product User's Guide, Operational Level 2 Data Versions 10 and Lite File Version 10 and VEarly, Technical Report National Aeronautics and Space Administration, Jet Propulsion Laboratory, California Institute of Technology, Pasadena, California, USA, Version 1.0, Revision A, June 8, 2020, Data Release: 10 (OCO-2), VEarly (OCO-3),

https://docserver.gesdisc.eosdis.nasa.gov/public/project/OCO/OCO2_OCO3_B10_DUG.pdf (last access: 17-Aug-2020), 2020.

Palmer, P. I., Feng, L., Baker, D., Chevallier, F., Bösch, H., and Somkuti, P.; Net carbon emissions from African biosphere
735   dominate pan-tropical atmospheric CO_2 signal, Nature Communications 10, Article number: 3344, pp. 9,
https://www.nature.com/articles/s41467-019-11097-w (last access: 15-July-2020), 2019.

Peters, W., Jacobson, A. R., Sweeney, C., Andrews, A. E., Conway, T. J., Masarie, K., Miller, J. B., Bruhwiler, L. M. P.
Pétron, G., Hirsch, A. I., Worthy, D. E. J., van der Werf, G. R.,Randerson, J. T., Wennberg, P. O., Krol, M. C., and Tans, P.
P.: An atmospheric perspective on North American carbon dioxide exchange: CarbonTracker, Proceedings of the National
740   Academy of Sciences (PNAS) of the United States of America, 104,18925–18930,doi:10.1073/pnas.0708986104, 2007.

Pillai, D., M. Buchwitz, C. Gerbig, T. Koch, M. Reuter, H. Bovensmann, J. Marshall, J. P. Burrows, Tracking city CO_2
emissions from space using a high resolution inverse modeling approach: A case study for Berlin, Germany, Atmos. Chem.
Phys., 16, 9591-9610, doi:10.5194/acp-16-9591-2016, 2016.

Pinty, B., Janssens-Maenhout, G., Dowell, M., Zunker, H., Brunhes, T., Ciais, P., Dee, D., Denier van der Gon, H., Dolman,
745   H., Drinkwater, M., Engelen, R., Heimann, M., Holmlund, K., Husband, R., Kentarchos, A., Meijer, Y., Palmer, P., and
Scholze, M.: An Operational Anthropogenic CO_2 Emissions Monitoring & Verification Support capacity - Baseline
Requirements, Model Components and Functional Architecture, doi: 10.2760/39384, European Commission Joint Research
Centre, EUR 28736 EN, pp. 102, https://www.copernicus.eu/sites/default/files/2019-09/CO2_Red_Report_2017.pdf (last
access: 26-Aug-2020), 2017.

750   Pinty, B., Ciais, P., Dee, D., Dolman, H., Dowell, M., Engelen, R., Holmlund, K., Janssens-Maenhout, G., Meijer, Y.,
Palmer, P., Scholze, M., Denier van der Gon, H., Heimann, M., Juvyns, O., Kentarchos, A., and Zunker, H.: An Operational
Anthropogenic CO_2 Emissions Monitoring & Verification Support Capacity – Needs and high level requirements for in situ
measurements, doi: 10.2760/182790, European Commission Joint Research Centre, EUR 29817 EN, pp. 77,
https://www.copernicus.eu/sites/default/files/2019-09/CO2_Green_Report_2019.pdf (last access: 26-Aug-2020), 2019.

755   Reuter, M., Buchwitz, M., Schneising, O., Heymann, J., Bovensmann, H., and Burrows, J. P.: A method for improved
SCIAMACHY CO_2 retrieval in the presence of optically thin clouds, Atmos. Meas. Tech., 3, 209-232, 2010.

Reuter, M., Bovensmann, H., Buchwitz, M., Burrows, J. P., Connor, B. J., Deutscher, N. M., Griffith, D. W. T., Heymann,
J., Keppel-Aleks, G., Messerschmidt, J., Notholt, J., Petri, C., Robinson, J., Schneising, O., Sherlock, V., Velazco, V.,
Warneke, W., Wennberg, P. O., and Wunch, D.: Retrieval of atmospheric CO_2 with enhanced accuracy and precision from
760   SCIAMACHY: Validation with FTS measurements and comparison with model results, J. Geophys. Res., 116, D04301,
doi:10.1029/2010JD015047, 2011.

Reuter, M., Buchwitz, M., Schneising, O., Hase, F., Heymann, J., Guerlet, S., Cogan, A. J., Bovensmann, H., and Burrows, J. P.: A simple empirical model estimating atmospheric CO_2 background concentrations, Atmos. Meas. Tech., 5, 1349-1357, 2012.

765 Reuter, M., Boesch, H., Bovensmann, H., Bril, A., Buchwitz, M., Butz, A., Burrows, J. P., O'Dell, C. W., Guerlet, S., Hasekamp, O., Heymann, J. , Kikuchi, N., Oshchepkov, S., Parker, R., Pfeifer, S., Schneising, O., Yokota, T., and Yoshida, Y.: A joint effort to deliver satellite retrieved atmospheric CO_2 concentrations for surface flux inversions: the ensemble median algorithm EMMA, Atmos. Chem. Phys., 13, 1771-1780, 2013.

Reuter, M., Buchwitz, M., Hilker, M., Heymann, J., Schneising, O., Pillai, D., Bovensmann, H., Burrows, J. P., Bösch, H., 770 Parker, R., Butz, A., Hasekamp, O., O'Dell, C. W., Yoshida, Y., Gerbig, C., Nehrkorn, T., Deutscher, N. M., Warneke, T., Notholt, J., Hase, F., Kivi, R., Sussmann, R., Machida, T., Matsueda, H., and Sawa, Y.: Satellite-inferred European carbon sink larger than expected, Atmos. Chem. Phys., 14, 13739-13753, 2014a.

Reuter, M., Buchwitz, M., Hilboll, A., Richter, A., Schneising, O., Hilker, M., Heymann, J., Bovensmann, H., and Burrows, J. P.: Decreasing emissions of NOx relative to CO_2 in East Asia inferred from satellite observations, Nature Geoscience, 28 775 Sept. 2014, doi:10.1038/ngeo2257, pp. 4, 2014b.

Reuter, M., Buchwitz, M., Schneising, O., Noël, S., Rozanov, V., Bovensmann, H., and Burrows, J. P.: A Fast Atmospheric Trace Gas Retrieval for Hyperspectral Instruments Approximating Multiple Scattering - Part 1: Radiative Transfer and a Potential OCO-2 XCO_2 Retrieval Setup, Remote Sens., 9, 1159, doi:10.3390/rs9111159, 2017a.

Reuter, M., Buchwitz, M., Schneising, O., Noël, S., Bovensmann, H., and Burrows, J. P.: A Fast Atmospheric Trace Gas 780 Retrieval for Hyperspectral Instruments Approximating Multiple Scattering - Part 2: Application to XCO_2 Retrievals from OCO-2, Remote Sens., 9, 1102, doi:10.3390/rs9111102, 2017b.

Reuter, M., Buchwitz, M., Hilker, M., Heymann, J., Bovensmann, H., Burrows, J. P., Houweling, S., Liu, Y., Nassar, R., Chevallier, F., Ciais, P., Marshall, J., and Reichstein, M.: How much CO_2 is taken up by the European terrestrial biosphere? Bull. Amer. Meteor. Soc. doi:10.1175/BAMS-D-15-00310.1, 24 April 2017, 665-671, 2017c.

785 Reuter, M., Buchwitz, M., Schneising, O., Krautwurst, S., O'Dell, C. W., Richter, A., Bovensmann, H., and Burrows, J. P.: Towards monitoring localized CO_2 emissions from space: co-located regional CO_2 and NO_2 enhancements observed by the OCO-2 and S5P satellites, Atmos. Chem. Phys., https://www.atmos-chem-phys.net/19/9371/2019/, 19, 9371-9383, 2019.

Reuter, M., Buchwitz, M., Schneising, O., Noel, S., Bovensmann, H., Burrows, J. P., Boesch, H., Di Noia, A., Anand, J., Parker, R. J., Somkuti, P., Wu, L., Hasekamp, O. P., Aben, I., Kuze, A., Suto, H., Shiomi, K., Yoshida, Y., Morino, I., Crisp, 790 D., O'Dell, C. W., Notholt, J., Petri, C., Warneke, T., Velazco, V. A., Deutscher, N. M., Griffith, D. W. T., Kivi, R., Pollard, D. F., Hase, F., Sussmann, R., Te, Y. V., Strong, K., Roche, S., Sha, M. K., De Maziere, M., Feist, D. G., Iraci, L. T., Roehl, C. M., Retscher, C., and Schepers, D.: Ensemble-based satellite-derived carbon dioxide and methane column-averaged dry-

air mole fraction data sets (2003-2018) for carbon and climate applications, Atmos. Meas. Tech., 13, 789-819, https://doi.org/10.5194/amt-13-789-2020, 2020.

795   Rodgers, C. D., Inverse Methods for Atmospheric Sounding: Theory and Practice, World Scientific Publishing, 2000.

Schneising, O., Buchwitz, M., Burrows, J. P., Bovensmann, H., Reuter, M., Notholt, J., Macatangay, R., and Warneke, T.: Three years of greenhouse gas column-averaged dry air mole fractions retrieved from satellite – Part 1: Carbon dioxide, Atmos. Chem. Phys., 8, 3827–3853, https://doi.org/10.5194/acp-8-3827-2008, 2008.

Schneising, O., Heymann, J., Buchwitz, M., Reuter, M., Bovensmann, H., and Burrows, J. P.: Anthropogenic carbon dioxide
800   source areas observed from space: assessment of regional enhancements and trends, Atmos. Chem. Phys., 13, 2445-2454, doi:10.5194/acp-13-2445-2013, 2013.

Schneising, O., Reuter, M., Buchwitz, M., Heymann, J., Bovensmann, H., and Burrows, J. P.: Terrestrial carbon sink observed from space: variation of growth rates and seasonal cycle amplitudes in response to interannual surface temperature variability, Atmos. Chem. Phys., 14, 133-141, 2014.

805   Schwandner, F. M., Gunson, M. R., Miller, C. E., Carn, S. A., Eldering, A., Krings, T., Verhulst, K. R., Schimel, D. S., Nguyen, H. M., Crisp, D., O'Dell, C. W., Osterman, G. B., Iraci, L. T., and Podolske, J. R.: Spaceborne detection of localized carbon dioxide sources, Science, 358, eaam5782, doi: 10.1126/science.aam5782, 2017.

Sussmann, R., and Rettinger, M.: Can We Measure a COVID-19-Related Slowdown in Atmospheric CO_2 Growth? Sensitivity of Total Carbon Column Observations, Remote Sens., 12, 2387, https://doi.org/10.3390/rs12152387 (last access:
810   10-Feb-2021), 2020.

Tohjima, Y., Patra, P.K., Niwa, Y., Mukai, H., Sasakawa, M., and Machida, T.: Detection of fossil-fuel CO_2 plummet in China due to COVID-19 by observation at Hateruma, Sci Rep 10, 18688, https://doi.org/10.1038/s41598-020-75763-6, 2020.

Veefkind, J. P., Aben, I., McMullan, K., Förster, H., De Vries, J., Otter, G., Claas, J., Eskes, H. J., De Haan, J. F., Kleipool, Q., Van Weele, M., Hasekamp, O., Hoogeveen, R., Landgraf, J., Snel, R., Tol, P.,Ingmann, P., Voors, R., Kruizinga, B.,
815   Vink, R., Visser, H., and Levelt, P. F.: TROPOMI on the ESA Sentinel-5 Precursor: A GMES mission for global observations of the atmospheric composition for climate, air quality and ozone layer applications. Rem. Sens. Environment, 120:70–83, 2012.

Velazco, V. A., M. Buchwitz, H. Bovensmann, M. Reuter, O. Schneising, J. Heymann, T. Krings, K. Gerilowski, and J. P. Burrows, Towards space based verification of CO_2 emissions from strong localized sources: fossil fuel power plant
820   emissions as seen by a CarbonSat constellation, Atmos. Meas. Tech., 4, 2809-2822, 2011.

Wu, L., Hasekamp, O., Hu, H., Landgraf, J., Butz, A., aan de Brugh, J., Aben, I., Pollard, D. F., Griffith, D. W. T., Feist, D. G., Koshelev, D., Hase, F., Toon, G. C., Ohyama, H., Morino, I., Notholt, J., Shiomi, K., Iraci, L., Schneider, M., de

Mazière, M., Sussmann, R., Kivi, R., Warneke, T., Goo, T.-Y., and Té, Y.: Carbon dioxide retrieval from OCO-2 satellite observations using the RemoTeC algorithm and validation with TCCON measurements, Atmos. Meas. Tech., 11, 3111–
825   3130, https://doi.org/10.5194/amt-11-3111-2018, 2018.

Wu, L., Aben, I., and Hasekamp, O. P.: Product User Guide and Specification (PUGS) – ANNEX B for products CO2_GOS_SRFP, CH4_GOS_SRFP (v2.3.8, 2009-2018), 29-Nov-2019, pp. 26, http://wdc.dlr.de/C3S_312b_Lot2/Documentation/GHG/PUGS/C3S_D312b_Lot2.3.2.3-v1.0_PUGS-GHG_ANNEX-B_v3.1.pdf (last access: 17-Aug-2020), 2019.

830   Wu, D., Lin, J., Oda, T., and Kort, E.: Space-based quantification of per capita CO_2 emissions from cities, Environ. Res. Lett. 15, pp. 9, https://iopscience.iop.org/article/10.1088/1748-9326/ab68eb/pdf (last access: 15-July-2020), 2020.

Wunch, D., Toon, G.C.,Wennberg, P.O.,Wofsy, S.C., Stephens, B.B., Fischer, M.L., Uchino, O., Abshire, J.B., Bernath, P., Biraud, S.C., Blavier, J.-F.L., Boone, C., Bowman, K.P., Browell, E.V., Campos, T., Connor, B.J., Daube, B.C., Deutscher, N.M., Diao, M., Elkins, J.W., Gerbig, C., Gottlieb, E., Griffith, D.W.T., Hurst, D.F., Jimenez, R., Keppel-Aleks, G., Kort,
835   E.A., Macatangay, R., Machida, T., Matsueda, H., Moore, F., Morino, I., Park, S., Robinson, J., Roehl, C.M., Sawa, Y., Sherlock, V., Sweeney, C., Tanaka, T., Zondlo, M.A.: Calibration of the total carbon column observing network using aircraft profile data. Atmos. Meas. Tech. 3:1351–1362. http://dx.doi.org/10.5194/amt-3-1351-2010, 2010.

Wunch, D., Toon, G. C., Blavier, J.-F. L., Washenfelder, R. A., Notholt, J., Connor, B. J., Griffith, D. W. T., Sherlock, V., and Wennberg, P. O.: The Total Carbon Column Observing Network. Phil. Trans. R. Soc. A, 369, 2087–2112,
840   doi:10.1098/rsta.2010.0240, 2011.

Wunch, D., Wennberg, P. O., Osterman, G., Fisher, B., Naylor, B., Roehl, C. M., O'Dell, C., Mandrake, L., Viatte, C., Kiel, M., Griffith, D. W. T., Deutscher, N. M., Velazco, V. A., Notholt, J., Warneke, T., Petri, C., De Maziere, M., Sha, M. K., Sussmann, R., Rettinger, M., Pollard, D., Robinson, J., Morino, I., Uchino, O., Hase, F., Blumenstock, T., Feist, D. G., Arnold, S. G., Strong, K., Mendonca, J., Kivi, R., Heikkinen, P., Iraci, L., Podolske, J., Hillyard, P. W., Kawakami, S.,
845   Dubey, M. K., Parker, H. A., Sepulveda, E., García, O. E., Te, Y., Jeseck, P., Gunson, M. R., Crisp, D., and Eldering, A.: Comparisons of the Orbiting Carbon Observatory-2 (OCO-2) XCO_2 measurements with TCCON, Atmos. Meas. Tech., 10, 2209-2238, do:10.5194/amt-10-2209-2017, 2017.

Wunch, D., Mendonca, J., Colebatch, O., Allen, N. T., Blavier, J.-F., Roche, S., Hedelius, J., Neufeld, G., Springett, S., Worthy, D., Kessler, R., and Strong, K.: TCCON data from East Trout Lake, SK (CA), Release GGG2014.R1. TCCON data
850   archive, hosted by CaltechDATA, https://doi.org/10.14291/tccon.ggg2014.easttroutlake01.R1, 2018.

Ye, X., Lauvaux, T., Kort, E. A., Oda, T., Feng, S., Lin, J. C., Yang, E. G., and Wu, D.: Constraining fossil fuel CO_2 emissions from urban area using OCO-2 observations of total column CO_2, Journal of Geophysical Research: Atmospheres, 125, e2019JD030528. https://doi.org/10.1029/2019JD030528, 2020.

Yin, Y., Ciais, P., Chevallier, F., Li, W., Bastos, A., Piao, S., Wang, T., and Liu, H.: Changes in the response of the Northern
Hemisphere carbon uptake to temperature over the last three decades. Geophysical Research Letters, 45, 4371– 4380,
https://doi.org/10.1029/2018GL077316, 2018to

Yoshida, Y., Kikuchi, N., Morino, I., Uchino, O., Oshchepkov, S., Bril, A., Saeki, T., Schutgens, N., Toon, G. C., Wunch,
D., Roehl, C. M., Wennberg, P. O., Griffith, D. W. T, Deutscher, N. M., Warneke, T., Notholt, J., Robinson, J., Sherlock, V.,
Connor, B., Rettinger, M., Sussmann, R., Ahonen, P., Heikkinen, P., Kyrö, E., Mendonca, J., Strong, K., Hase, F., Dohe, S.,
and Yokota, T.: Improvement of the retrieval algorithm for GOSAT SWIR XCO_2 and XCH_4 and their validation using
TCCON data, Atmos. Meas. Tech., 6, 1533–1547, doi:10.5194/amt-6-1533-2013, 2013.

Zhang, R., Zhang, Y., Lin, H., Feng, X., Fu, T.-M., and Wang, Y.: NOx Emission Reduction and Recovery during
COVID-19 in East China, Atmosphere, 11, 433, pp. 15, doi:10.3390/atmos11040433, 2020.

Zheng, B., Chevallier, F., Ciais, P., Broquet, G., Wang, Y., Lian, J., and Zhao, Y.: Observing carbon dioxide emissions over
China's cities and industrial areas with the Orbiting Carbon Observatory-2, Atmos. Chem. Phys., 20, 8501–8510,
https://doi.org/10.5194/acp-20-8501-2020 (last access: 5-Jan-2021), 2020a.

Zheng, B., Geng, G., Ciais, P., Davis, S. J., Martin, R. V., Meng, J., Wu, N., Chevallier, F., Broquet, G., Boersma, F., van
der A, R., Lin, J., Guan, D., Lei, Y., He, K., and Zhang, Q.: Satellite-based estimates of decline and rebound in China's CO_2
emissions during COVID-19 pandemic. Sci. Adv. 6, eabd4998, https://advances.sciencemag.org/content/6/49/eabd4998 (last
access: 5-Jan-2021), 2020b.

Zeng, N., Han, P., Liu, D., Liu, Z., Oda, T., Martin, C., Liu, Z., Yao, B., Sun, W., Wang, P., Cai, Q., Dickerson, R., and
Maksyutov, S.: Global to local impacts on atmospheric CO_2 caused by COVID-19 lockdown, pp. 20,
https://arxiv.org/abs/2010.13025 (last access: 5-Jan-2021), 2020.

Tables:

Table 1. Overview of the satellite XCO₂ Level 2 (L2) input data products. (#) Products are available via the Copernicus Climate Data Store (CDS, https://cds.climate.copernicus.eu/cdsapp#!/dataset/satellite-carbon-dioxide?tab=overview (last access: 23-September-2020)) currently until end of 2019. Year 2020 data will be made available via the CDS in mid 2021 but are available

 from the authors on request (see contact information).

Satellite	Algorithm	Product version	Product ID	References	Data provider and data access information
OCO-2	ACOS	v10r	CO2_OC2_ACOS	O'Dell et al., 2018; Kiel et al., 2019; Osterman et al., 2020	Product "OCO2_L2_Lite_FP 10r" obtained from NASA's Earthdata GES DISC website: https://disc.gsfc.nasa.gov/datasets?keywords=OCO-2%20v10r&page=1 (last access: 15-Aug-2020)
GOSAT	UoL-FP	v7.3	CO2_GOS_OCFP	Cogan et al., 2012; Boesch et al., 2019	Generated by Univ. Leicester (contact: Antonio Di Noia: adn9@leicester.ac.uk) and available via the CDS (#)
GOSAT	RemoTeC	v2.3.8	CO2_GOS_SRFP	Butz et al., 2011; Wu et al., 2019	Generated by SRON (contact: Lianghai Wu: L.Wu@sron.nl) and available via the CDS (#)
GOSAT	FOCAL	v1.0	CO2_GOS_FOCA	Noël et al., 2020	Generated by Univ. Bremen and available on request (contact: Stefan Noël: Stefan.Noel@iup.physik.uni-bremen.de)

Table 2. Overview of the CarbonTracker CT2019 data set. For this study we used data from the period January 2015 to December 885 2018.

Model / Version	Details	Reference	Access
CarbonTracker CT2019	Atmospheric CO_2 molefraction profiles (spatio-temporal sampling: 3°x2°, 3-hourly) and CO_2 fluxes (spatio-temporal sampling: 1°x1°, 3-hourly)	Jacobson et al., 2020 DOI: http://dx.doi.org/10.25925/39m3-6069 (last access: 22-July-2020)	CarbonTracker CT2019, http://carbontracker.noaa.gov (last access: 22-July-2020)

890

Table 3. Corner coordinates of the East China target region as analysed in this study.

Region ID	Comments	Latitude range [deg North]	Lontitude range [deg East]
East China	Target region for DAM and TmS methods	28 – 44	102 – 126
	Extended region for TmS method	18 -54	93 - 135

895

Table 4. Numerical values of the ensemble-based $CO_2^{FF(DAM)}$ results as shown in Fig. 13. Listed are the median values and corresponding 1-sigma uncertainties (in brackets). The dimensionless values listed here represent the relative $CO_2^{FF(DAM)}$ change for January-May 2020 relative to October-December 2019 and previous years ("OND" anomalies, see main text).

900

Month Product ID	October 2019	November 2019	December 2019	January 2020	February 2020	March 2020	April 2020	May 2020
CO2_OC2_ACOS	-0.004 (0.025)	0.001 (0.024)	-0.010 (0.015)	0.008 (0.026)	-0.010 (0.024)	-0.003 (0.020)	-0.018 (0.023)	-0.019 (0.027)
CO2_GOS_OCFP	-0.049 (0.046)	0.026 (0.038)	0.071 (0.050)	-0.110 (0.077)	-0.055 (0.087)	-0.151 (0.101)	-0.281 (0.055)	-0.141 (0.158)
CO2_GOS_SRFP	-0.076 (0.031)	0.111 (0.030)	-0.061 (0.054)	0.038 (0.101)	-0.064 (0.053)	0.011 (0.081)	-0.082 (0.059)	0.024 (0.077)
CO2_GOS_FOCA	-0.057 (0.042)	0.053 (0.029)	0.008 (0.040)	-0.044 (0.062)	0.046 (0.081)	-0.176 (0.066)	-0.041 (0.069)	-0.080 (0.064)
Ensemble	-0.047 (0.031)	0.048 (0.047)	0.002 (0.054)	-0.027 (0.065)	-0.021 (0.050)	-0.085 (0.091)	-0.106 (0.120)	-0.054 (0.072)

Figures:
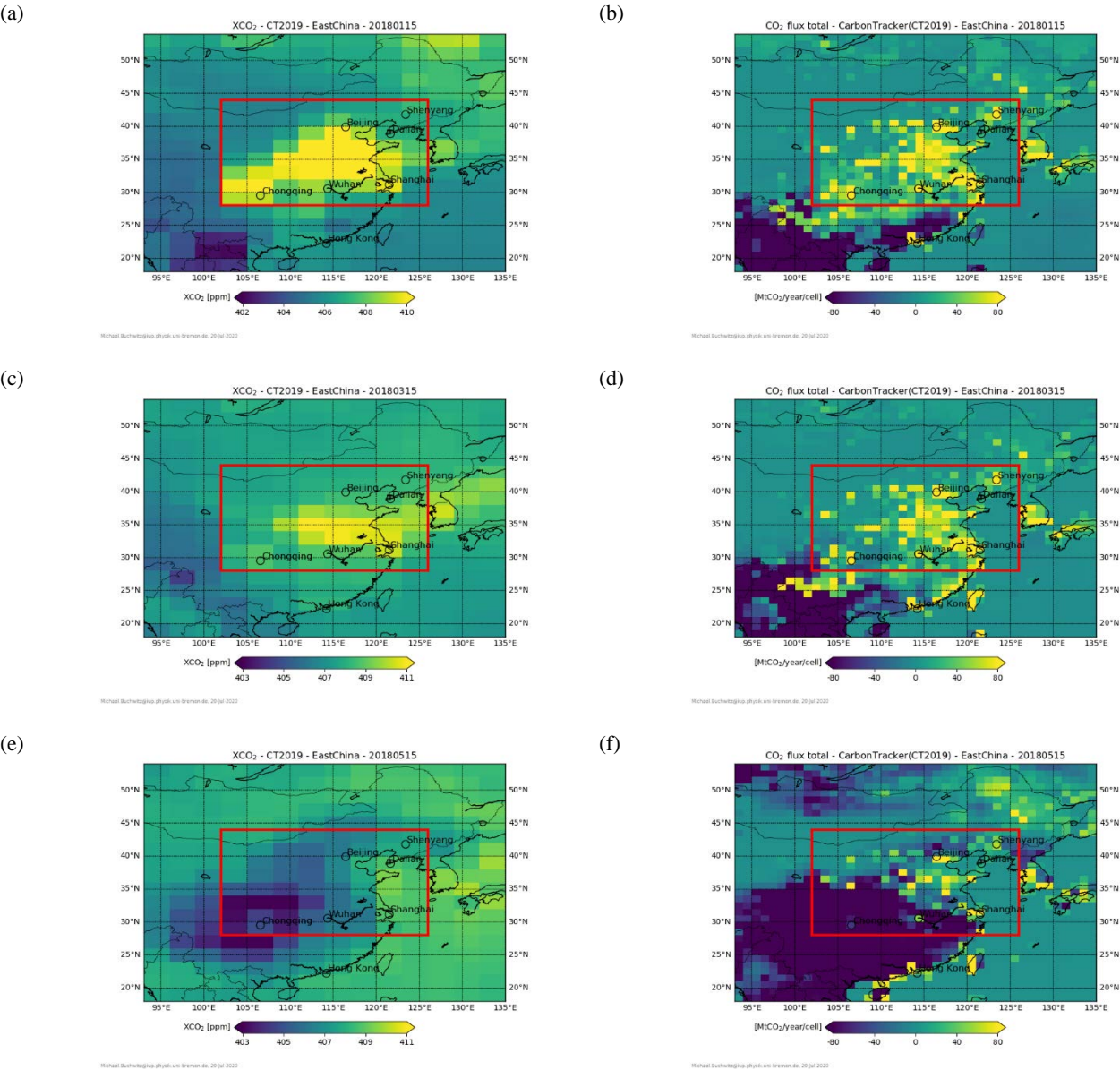
Figure 1: Left: CT2019 XCO₂ (left, in ppm) and corresponding CO₂ surface fluxes (right, in MtCO₂/year/cell) for 15-Jan-2018 (first row), 15-Mar-2018 (middle) and 15-May-2018 (bottom). The red rectangle encloses the East China target region as defined for this study.
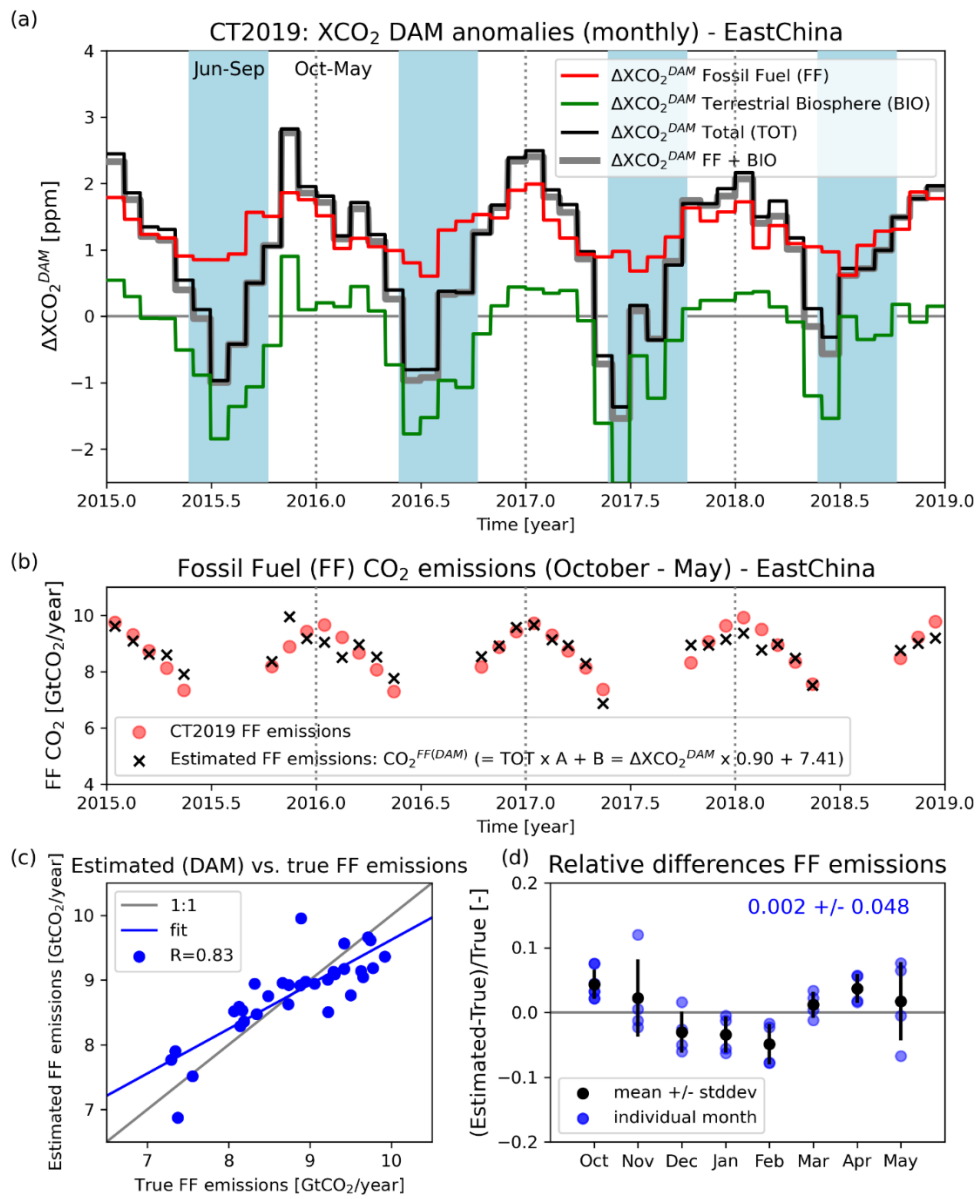
Figure 2: Results obtained by applying the DAM method to CT2019 XCO₂ for East China. (a): Different monthly ΔXCO_2^{DAM} components: Total ΔXCO_2^{DAM} (TOT) and its FF (red) and biogenic (BIO, green) components and their sum (FF + BIO). The non-shaded time periods October to May indicate the periods analysed in this publication. (b) East China October to May FF CO₂ emissions (red dots) and estimated emissions $CO_2^{FF(DAM)}$ (black crosses) as obtained from total ΔXCO_2^{DAM} (TOT as shown in panel (a)) using the formula shown in (b). (c) Scatter plot of estimated versus true (i.e., CT2019) FF emissions. (d) Relative difference of estimated and true emissions.
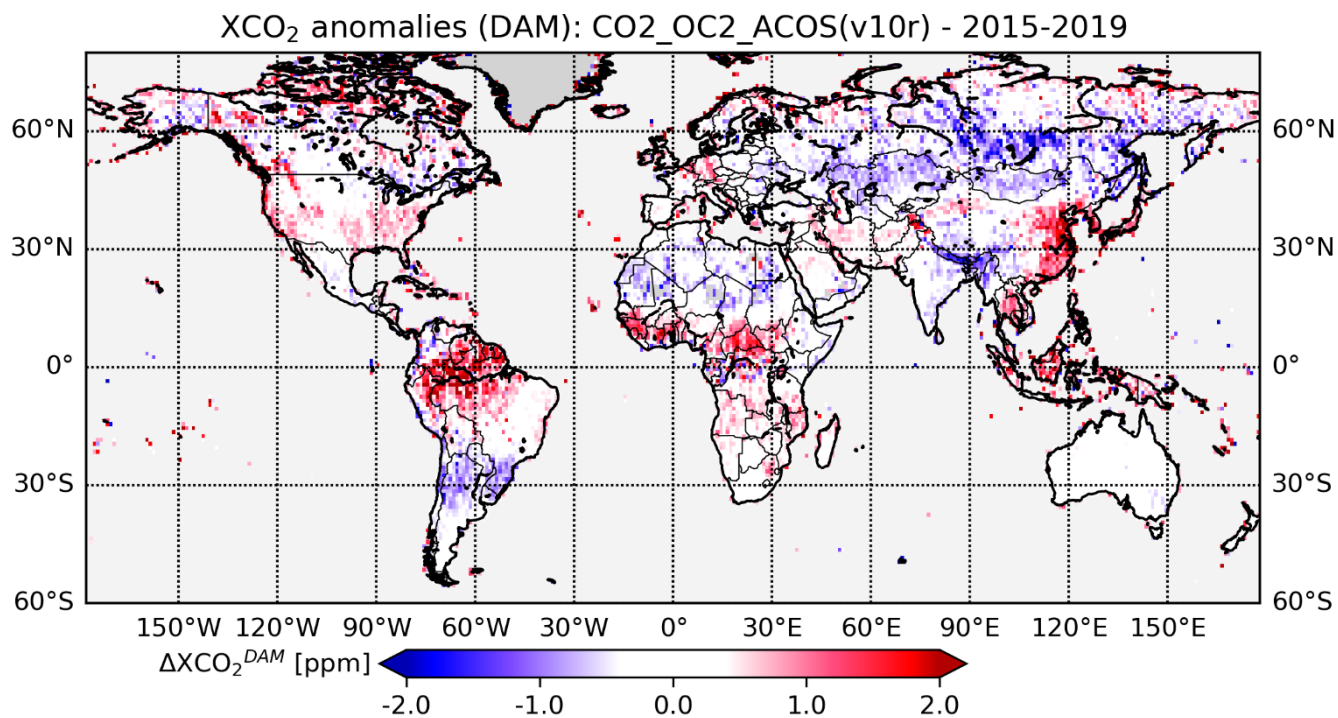
920

Figure 3: DAM XCO₂ anomaly map at 1º x 1º resolution generated from OCO-2 Level 2 XCO₂ (v10r, land) for 2015 to 2019.

925
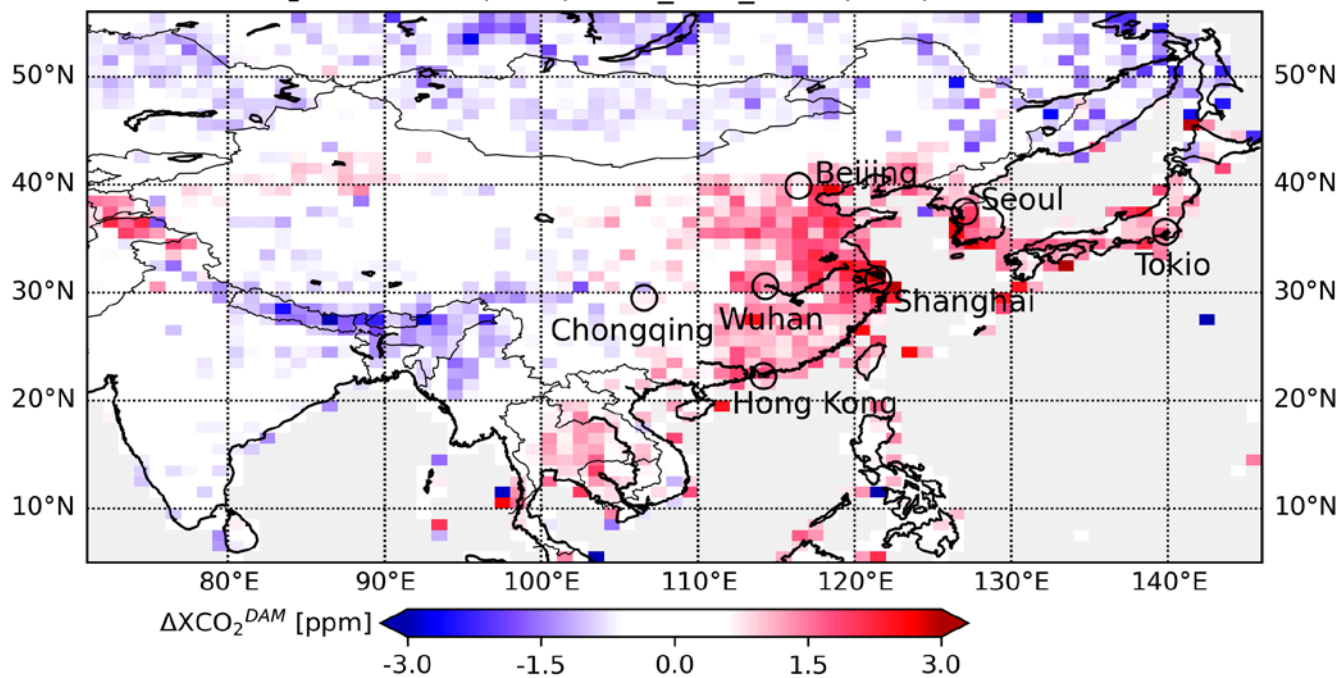
Figure 4: As Fig. 3 but for China and surrounding areas.
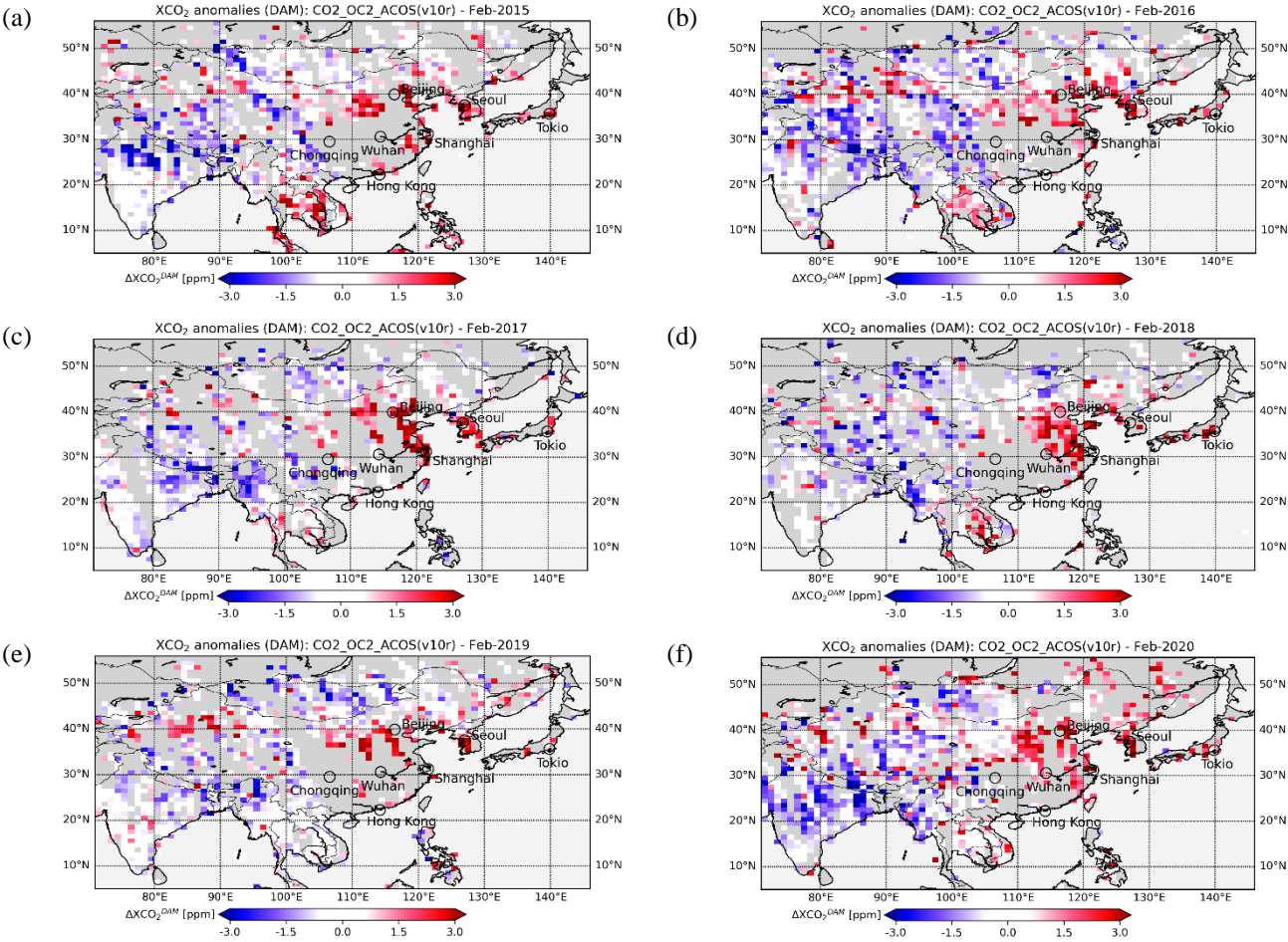
Figure 5: As Fig. 4 but for (a) February 2015 to (f) February 2020.
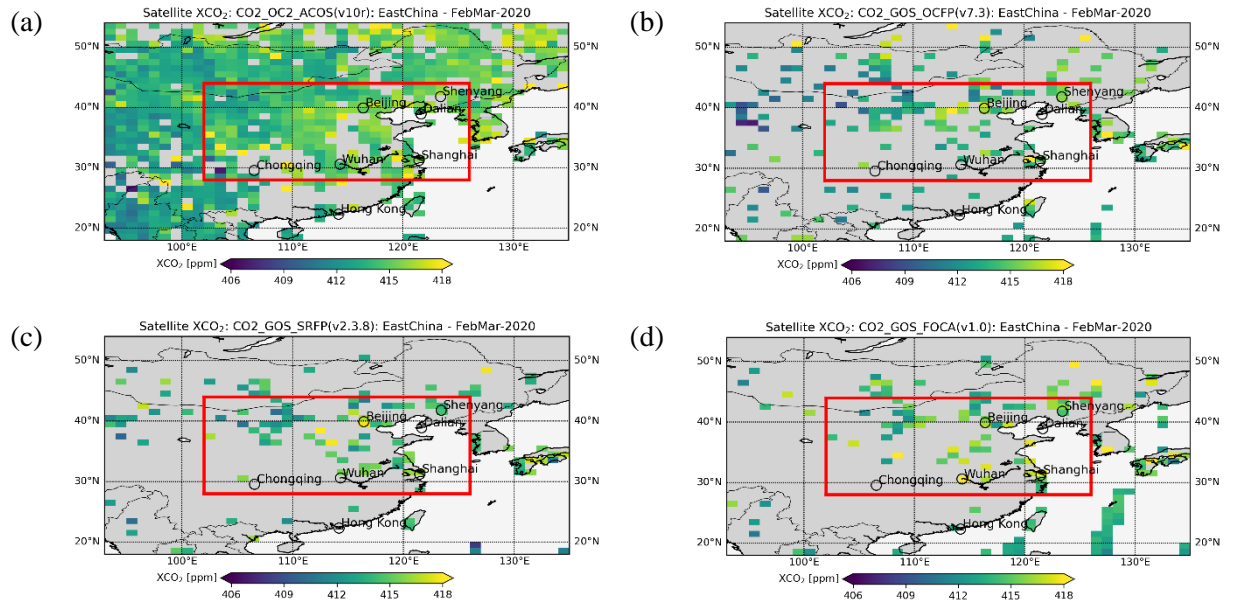
Figure 6: Panel (a): OCO-2 XCO₂ (version 10r, product ID CO2_OC2_ACOS) over land at 1°x1° resolution for February-March 2020. The red rectangle encloses the investigated East China target region. Panels (b)-(d) as panel (a) but for products CO2_GOS_OCFP (b), CO2_GOS_SRFP (c), and CO2_GOS_FOCA (d) (see Tab. 1 for details).
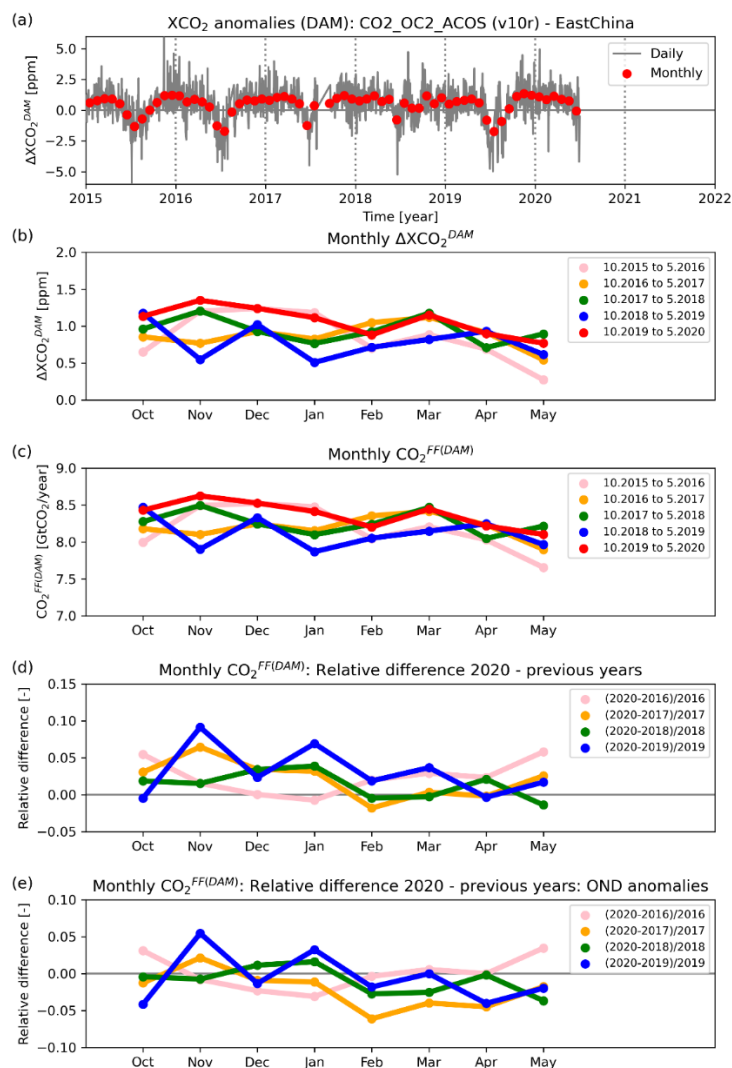
940

945

Figure 7: DAM analysis of the OCO-2 ACOS version 10r XCO_2 product (CO2_OC2_ACOS) for the region East China from January 2015 to May 2020. (a) The thin grey line shows the daily DAM XCO_2 anomalies, i.e., daily ΔXCO_2^{DAM}. The red dots are the corresponding monthly values, which are also shown in (b) for different October – May periods. (c) As (b) but for $CO_2^{FF(DAM)}$, i.e., for the estimated East China monthly FF emissions (see main text). The data for October 2019 – May 2020 (10.2019-5.2020) are shown in red (see annotation for other periods). (d) Relative $CO_2^{FF(DAM)}$ differences for different periods. In blue, for example, the differences correspond to the period 10.2019-5.2020 (shown in red in panel (c)) minus 10.2018-5.2019 (shown in blue in (c)). (e) As (d) but after the October to December mean value ("OND anomalies"). The following parameters have been used to generate this figure: Minimum number of observations/day: 30, minimum number of days/month: 5.
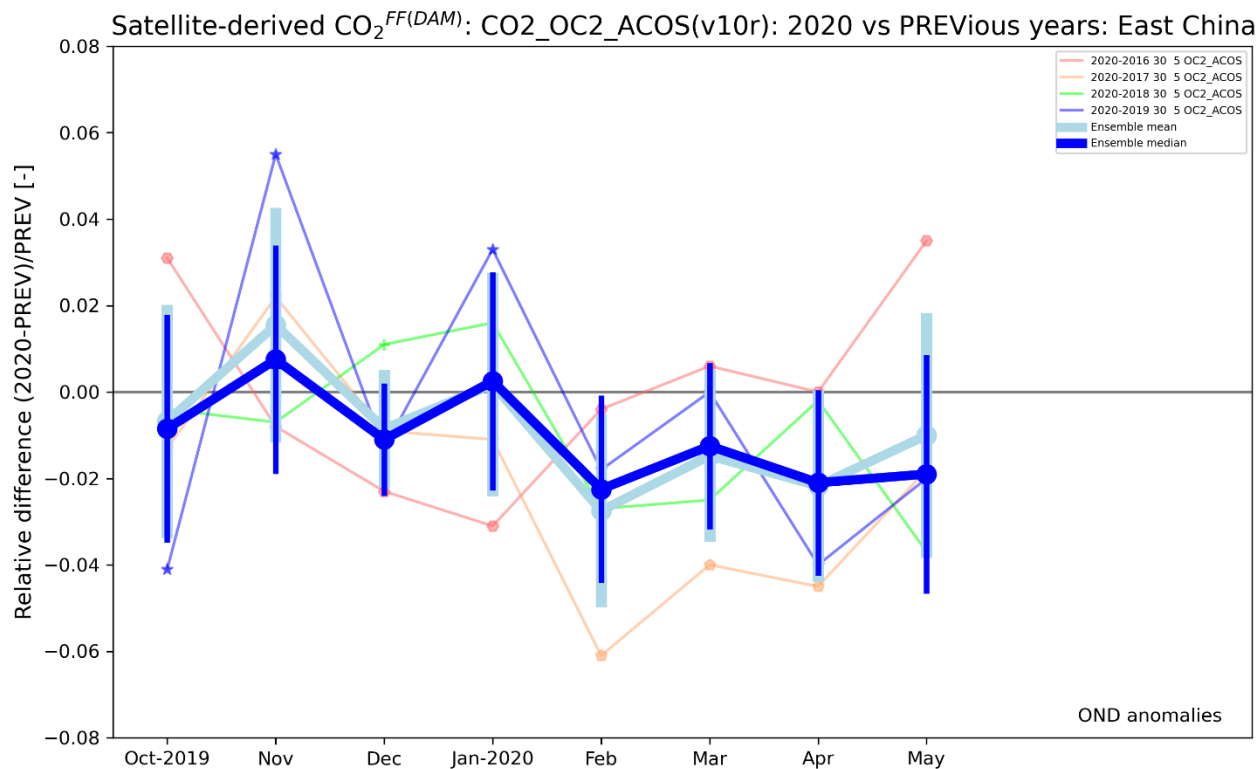
Satellite-derived CO$_2$$^{FF(DAM)}$: CO2_OC2_ACOS(v10r): 2020 vs PREVious years: East China

955 Michael.Buchwitz@iup.physik.uni-bremen.de, 29-January-2021

Figure 8: Ensemble members CO$_2$$^{FF(DAM)}$ OND anomalies derived from satellite product CO2_OC2_ACOS. The thin lines and small symbols show the same data also shown in the bottom panel of Fig. 7. The thick dots and lines show the corresponding ensemble median, mean and scatter. The following parameters have been used to generate this figure (see also annotation): Minimum number
960 **of observations/day: 30; minimum number of days/month: 5.**
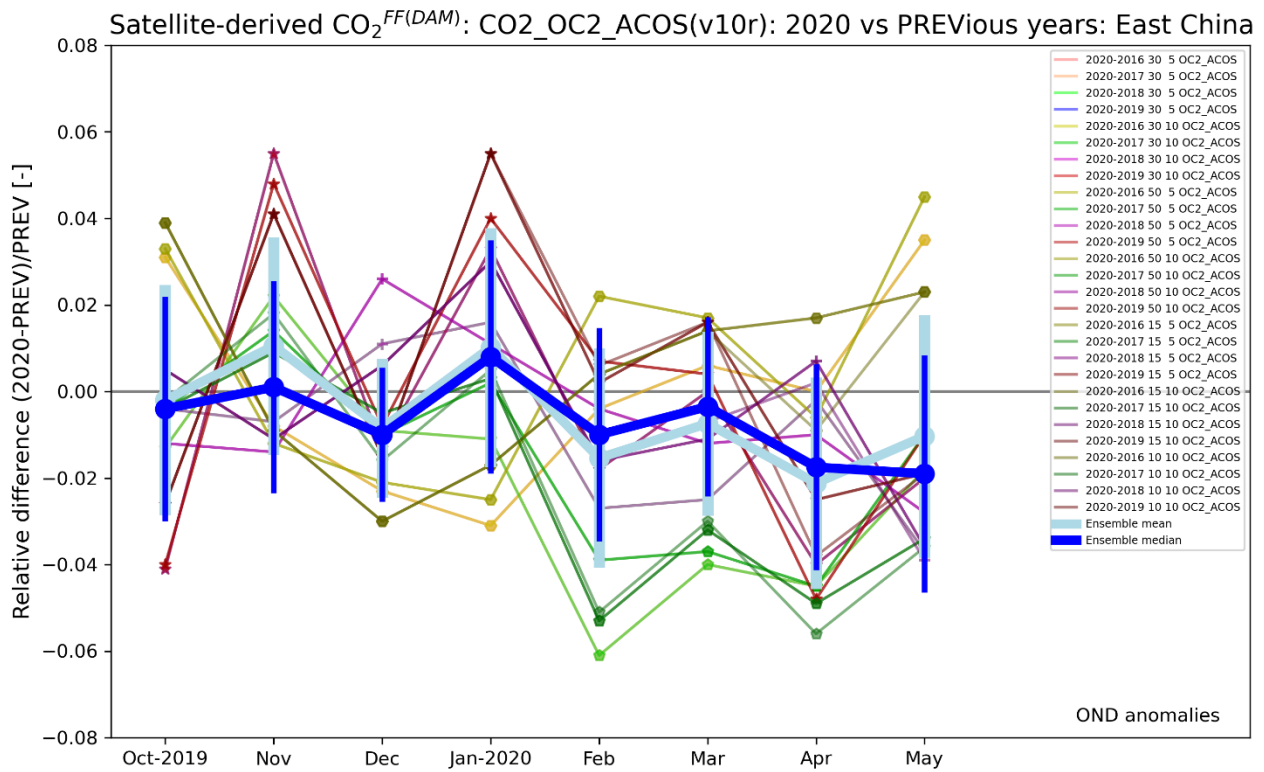
965 Michael.Buchwitz@iup.physik.uni-bremen.de, 29-January-2021

Figure 9: The same as Fig. 8 but with additional combinations of minimum number of observations/day (30 as in Fig. 8 and in addition: 50, 15 and 10) and minimum number of days/month (5 as in Fig. 8 and in addition 10) (see annotation).

Figure 10: The same as Figs. 9 but for the product CO2_GOS_OCFP. Results are shown for several values of the required minimum

 number of observations/day: 2, 4, 6, 8, 10 and 15. The required minimum number of days/month is 5.
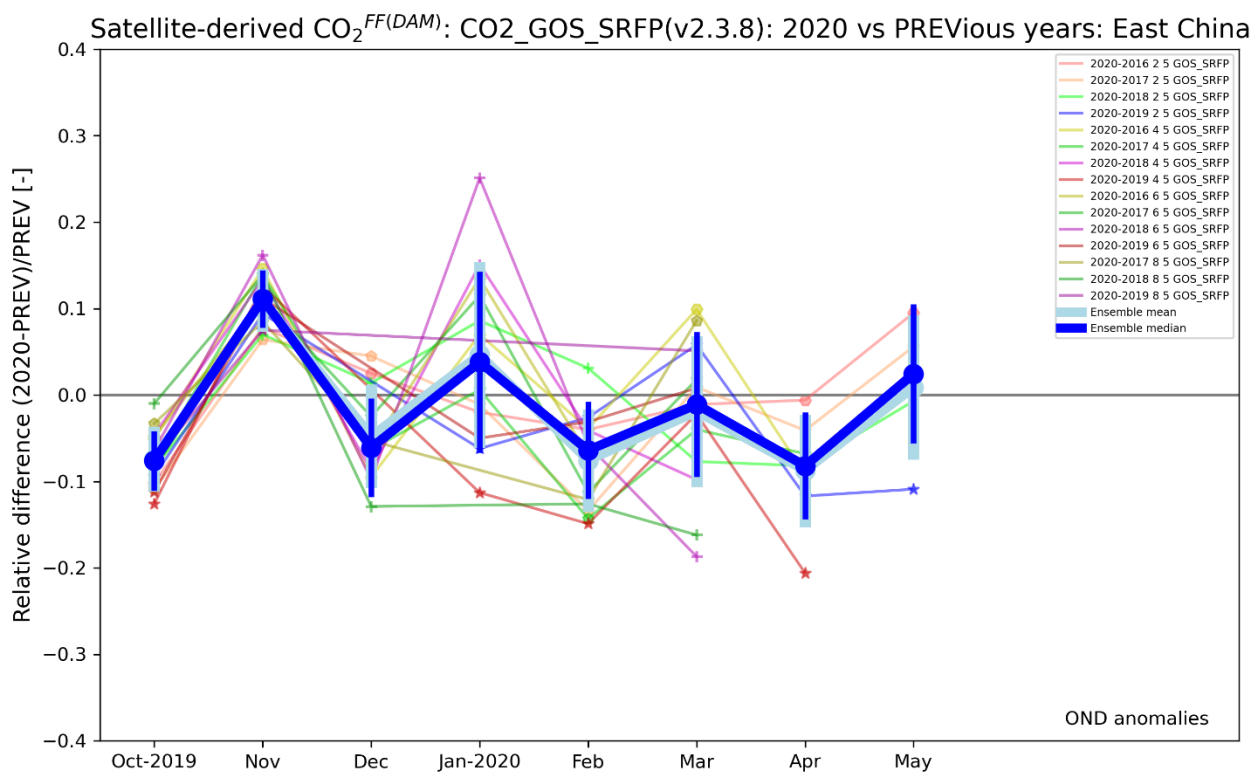
980   Michael.Buchwitz@iup.physik.uni-bremen.de, 29-January-2021

Figure 11: The same as Fig. 10 but for the product CO2_GOS_SRFP.
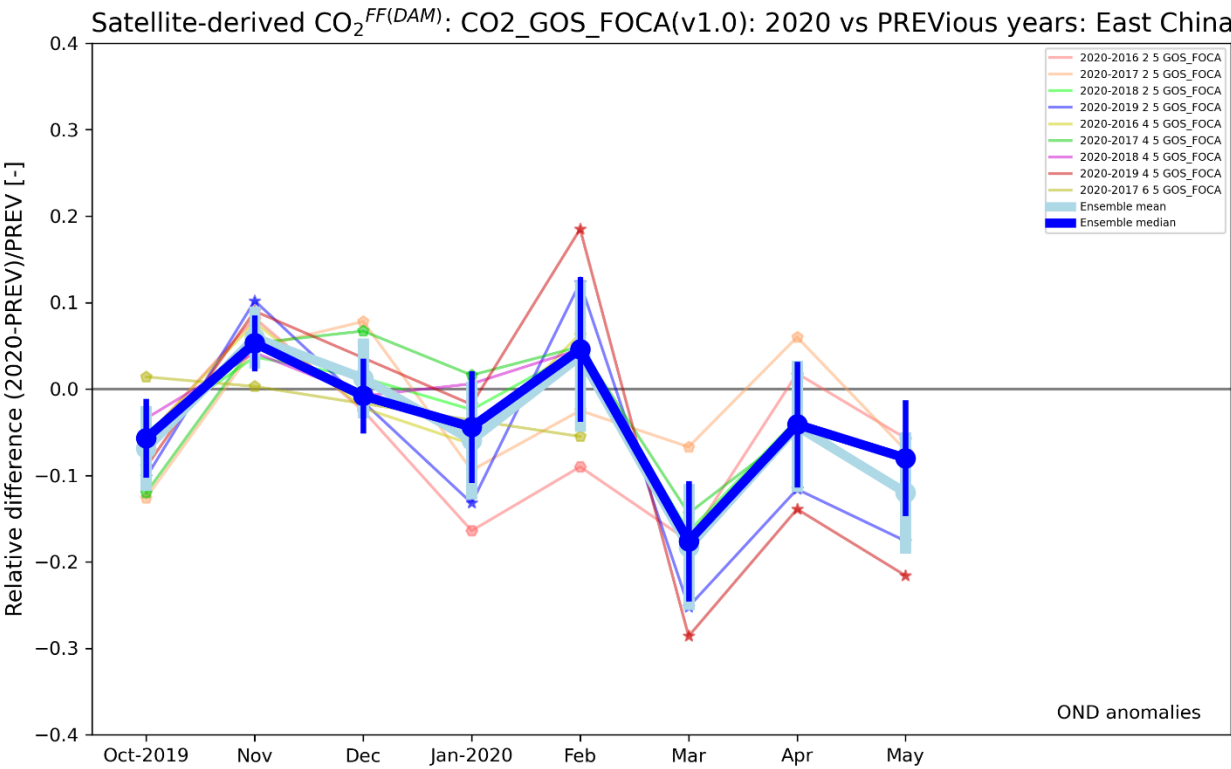
Figure 12: The same as Fig. 10 but for the product CO2_GOS_FOCA.
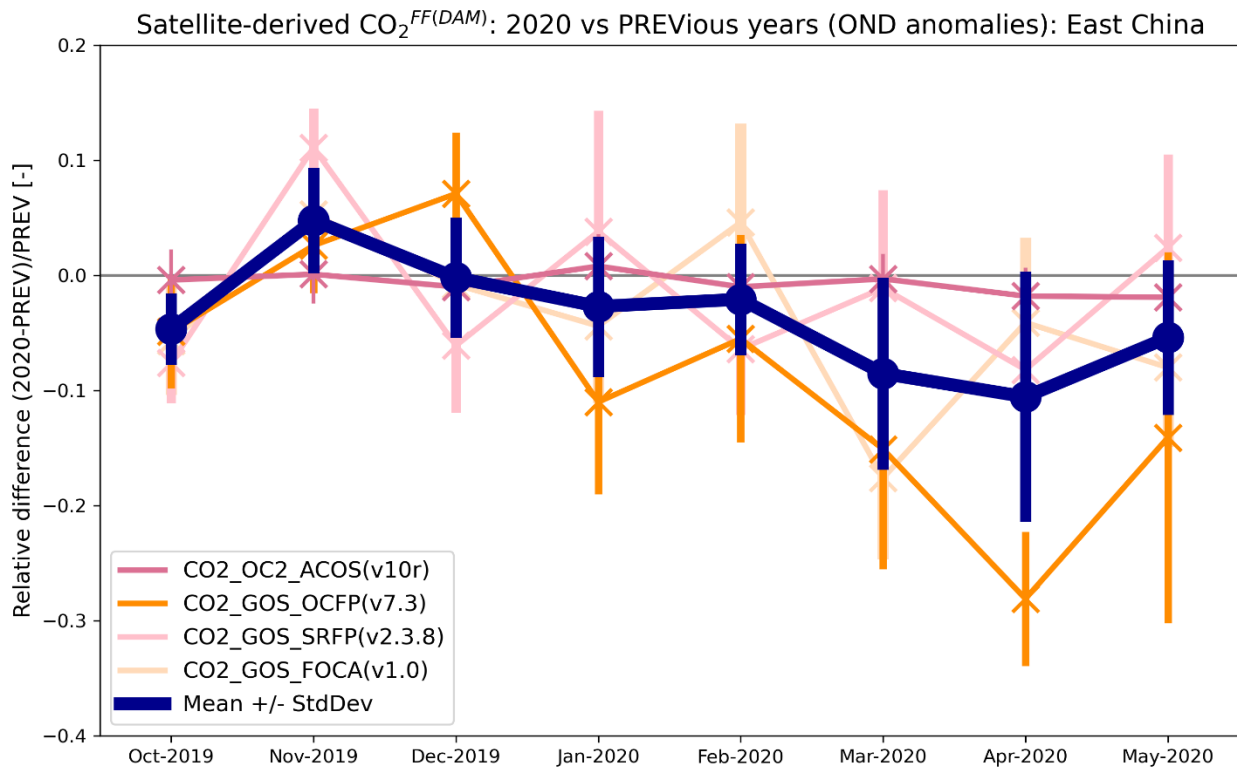
Michael.Buchwitz@iup.physik.uni-bremen.de, 1-February-2021

995 **Figure 13: Overview of the ensemble-based CO₂ FF(DAM) results for January-May 2020 relative to October-December 2019 and previous years (also shown in Figs. 9 – 12) via reddish colours for each of the four analysed satellite XCO₂ data products (see Tab. 1). The corresponding ensemble mean value and its uncertainty is shown in dark blue. The uncertainty has been computed as standard deviation of the ensemble members. The corresponding numerical values of the ensemble members are listed in Tab. 4.**

1000
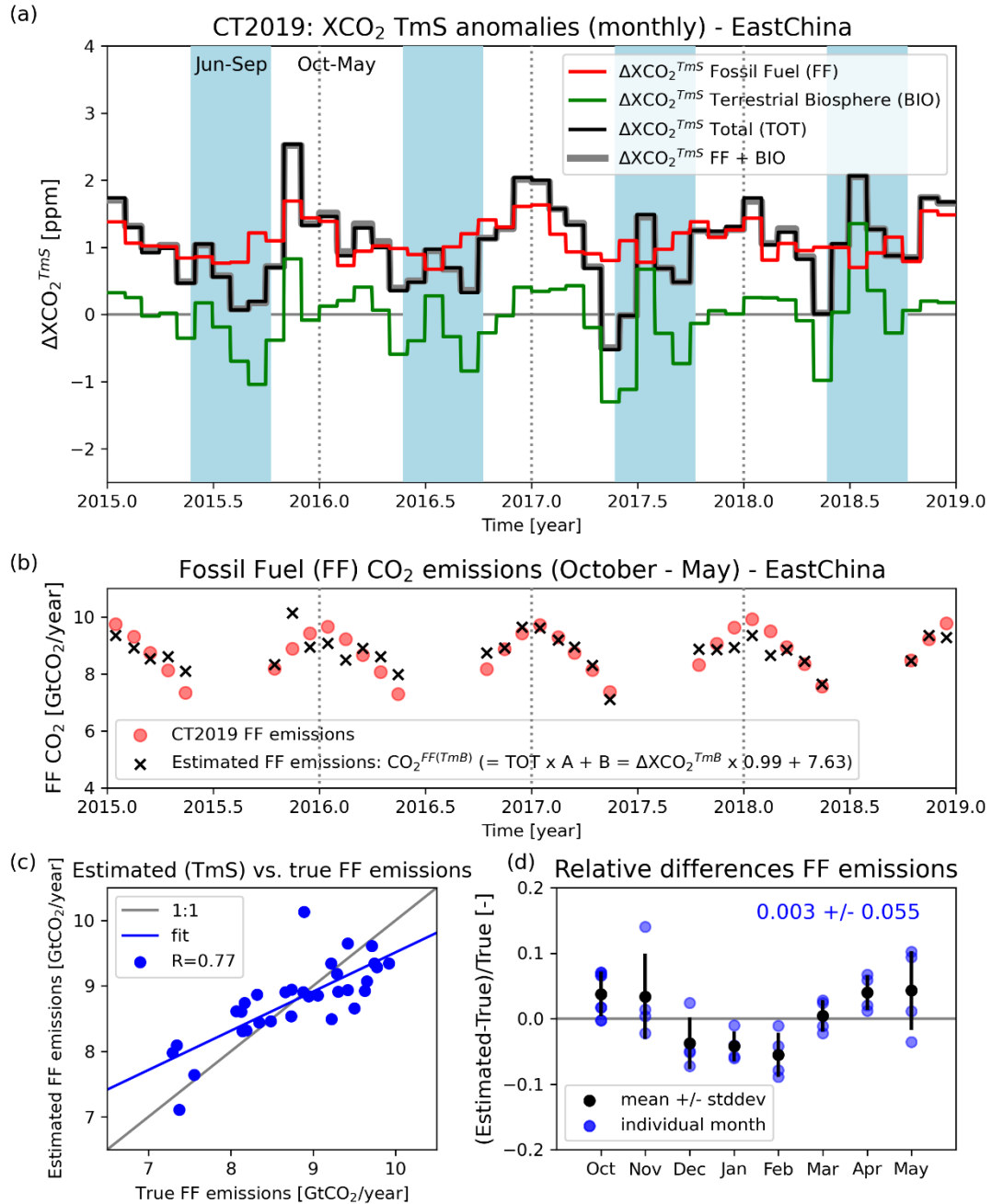
Michael.Buchwitz@iup.physik.uni-bremen.de, 28-January-2021

Figure A1: The same as Fig. 2 but using the Target minus Surrounding (TmS) method.
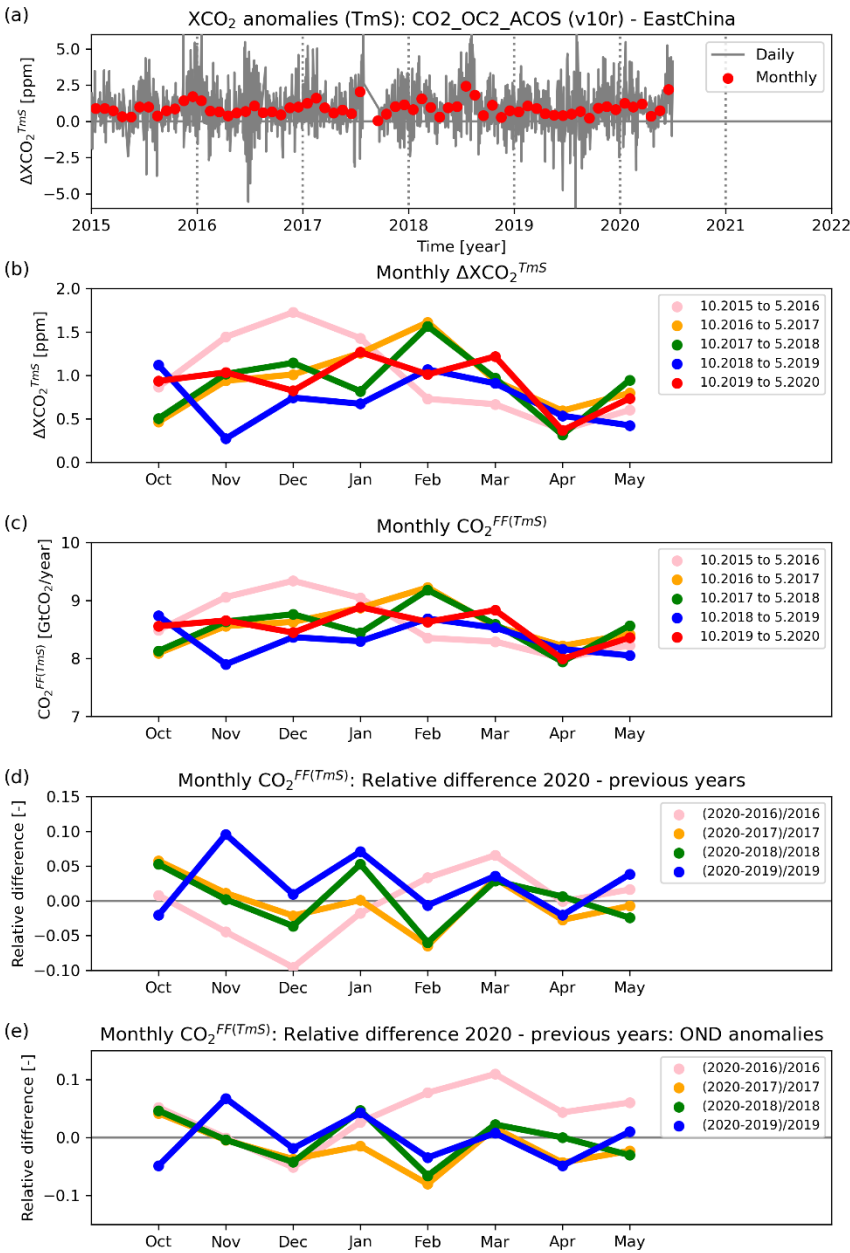
Figure A2: The same as Fig. 7 but using the TmS method.

Michael.Buchwitz@iup.physik.uni-bremen.de, 1-February-2021
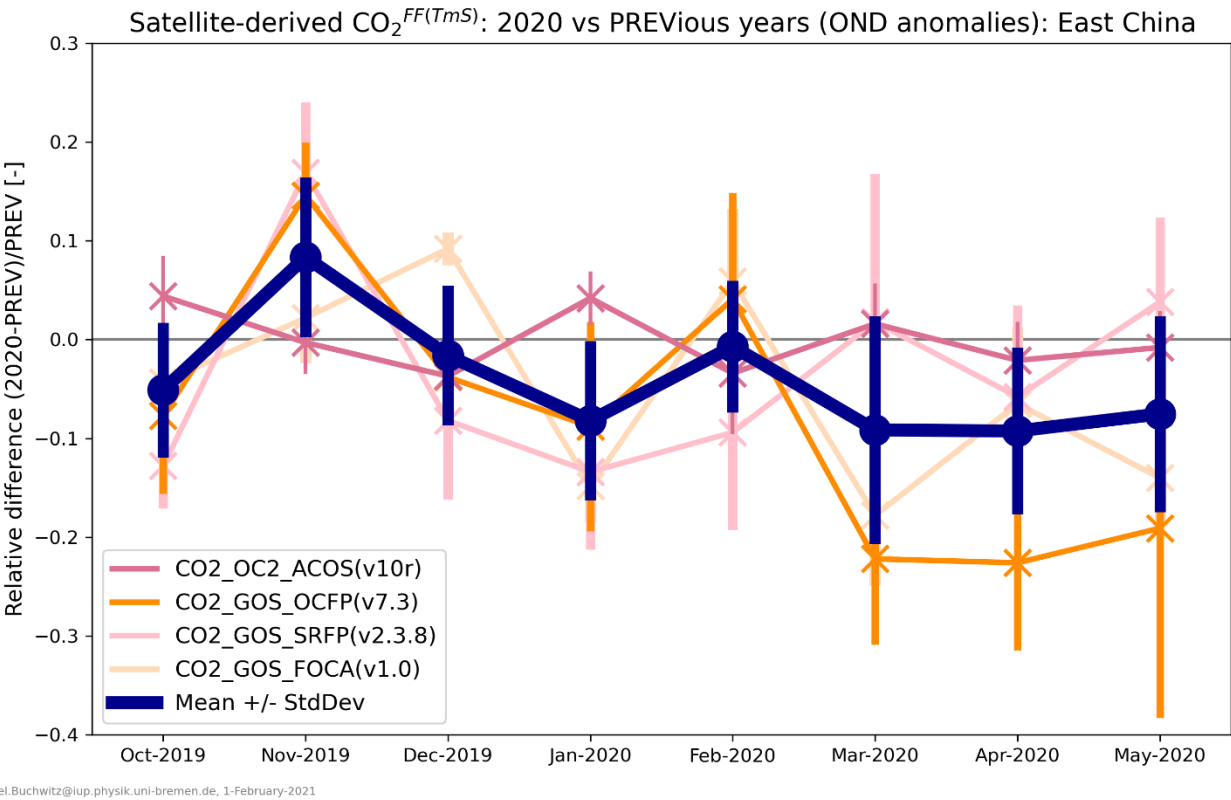
Figure A3: The same as Fig. 13 but using the TmS method.